NIKHEF PROJECT PLAN: CRYOLINKS
Cryogenic vacuum links to isolate interferometer arms for Advanced Virgo

Responsible: J.F.J. van den Brand[1],
[1] *Nikhef, National Institute for Subatomic Physics,*
P.O. Box 41882, Amsterdam, the Netherlands

June 3, 2010

email address: jo@nikhef.nl

Procedure start date	01/10/2009
Procedure end date	01/10/2013
Document version	v01r01
Version date	11/09/2009

Abstract

The current Virgo vacuum level needs to be improved by about a factor of hundred in order to be compliant with the required Advanced Virgo sensitivity. Such an improvement requires baking out the interferometer arms. To separate these arms from the towers that hold the mirrors and allow the bake-out, four cryogenic vacuum links will be installed.

Project collaborators

Name	Institution	email
Jo van den Brand (project leader)	Nikhef	jo@nikhef.nl
Martin Doets (project coordinator)	Nikhef	martind@nikhef.nl
Eric Hennes	Nikhef	e.hennes@science.uva.nl
Marco Kraan	Nikhef	marcok@science.uva.nl
Krista de Roo	Nikhef	kderoos@science.uva.nl
Richard Rosing	Nikhef	rrosing@science.uva.nl
Herman Boer Rookhuizen	Nikhef	hermanbr@nikhef.nl
Michiel Jaspers	Nikhef	y67@nikhef.nl
Willem Kuilman	Nikhef	y21@nikhef.nl
Vacuum engineer	Nikhef	vac@nikhef.nl
Electronic engineer	Nikhef	elec@nikhef.nl
Software engineer	Nikhef	soft@nikhef.nl
Antonio Pasqualetti (AdV VAC project leader)	EGO	antonio.pasqualetti@ego-gw.it
Gaelle Parguez	EGO	gaelle.parguez@ego-gw.it
Frederic Richard	EGO	frederic.richard@ego-gw.it
Carlo Bradaschia	Pisa	carlo.bradaschia@pi.infn.it
Irene Fiori	Pisa	irene.fiori@pi.infn.it
Violette Brisson	LAL	brisson@lal.in2p3.fr
Andrea Chincarini	Genua	Andrea.Chincarini@ge.infn.it
Gianluca Gemme	Genua	Gianluca.gemme@ge.infn.it
Jean-Yves Vinet	Nice	jean-yves.vinet@obs-nice.fr

Contents

1 Introduction

The enhancement of the Virgo sensitivity by a factor of 10 requires an improvement of the present vacuum level to lower the phase noise for YAG light scattering from the residual gas inside the 3 km long interferometer (ITF) arms. At present the system operates at about 10^{-7} mbar (dominated by water) although it has been designed and tested to reach a base pressure below 10^{-9} mbar (dominated by hydrogen) after an overall bakeout. A typical spectrum of gases recently taken in the Virgo West arm is reported in Fig. 1. The lowest point of the

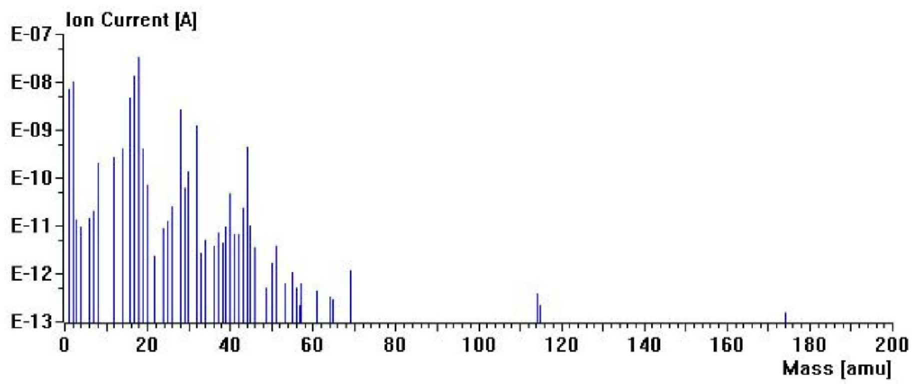

Figure 1: A recent measurement of the residual gas composition in the West-arm. The horizontal axis reports the ratio mass/charge of the ions and the vertical axis the corresponding ionization current which is proportional to the partial pressure. The dominant peak is the one at mass 18, water. Total pressure is about 10^{-7} mbar.

Advanced Virgo (AdV) sensitivity curve: $3 \times 10^{-24}/\sqrt{\text{Hz}}$ at 200 - 400 Hz is not compatible with the present residual gas phase noise, as shown by Fig. 2. Taking into account all the main

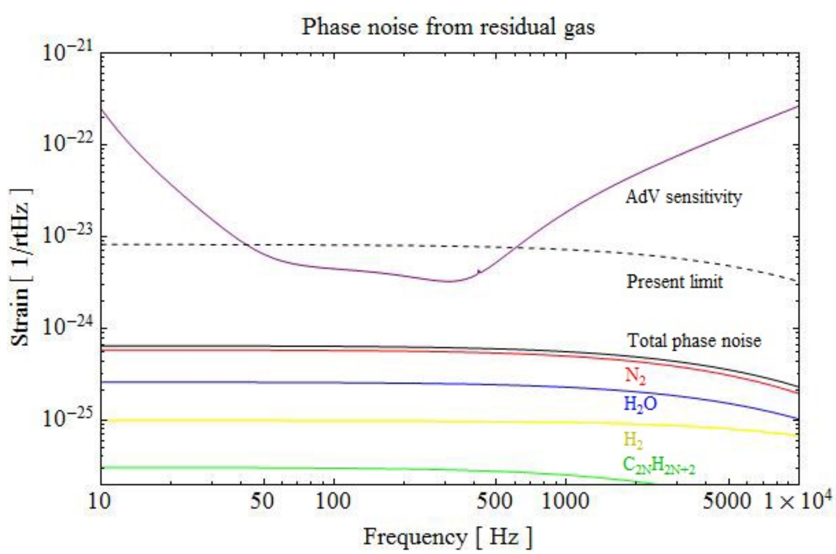

Figure 2: Advanced Virgo sensitivity curve (purple), phase noise contribution as it would be with the present vacuum level, due to water at a partial presure of 1.5×10^{-7} mbar (dashed curve). The sensitivity would be limited to about $10^{-23}/\sqrt{\text{Hz}}$. The green, yellow, blue and red curves represent the phase noise due to hydrocarbons, hydrogen, water vapor and nitrogen, respectively. Partial pressures are given in Table 1.1. The solid black curve shows the total expected contribution of phase noise that can be obtained with the cryolinks.

species composing the residual gas at the presently attained pressure, the corresponding noise is at the level of $10^{-23}/\sqrt{\text{Hz}}$. To be compatible with the requirements for AdV, this noise has to be reduced by at least a factor of 10 (about a factor of three below the AdV design sensitivity). The residual pressure in the ITF arms has to be reduced by a factor of 100, since the noise is proportional to the square root of the partial pressure of the various gas species (see below).

The selected technique to meet the proposed goal is:

- installing cryogenic links at the interferometer arm extremities;
- performing a bake-out of the ITF arms only.

Cryogenic links are the classical solution to stop the migration of water from unbaked towers to the ITF arms. In the present Virgo configuration, during the restart procedure after opening the towers to service mirrors or suspension systems, the gas released from these towers (mostly water vapor) spreads in the ITF arms, bringing temporarily the residual pressure near 10^{-6} mbar, orders of magnitude above our goal.

Virgo has already experimented with cryolinks, while also LIGO has cryolinks installed on their interferometer. Therefore, we aim at installing cryolinks in Advanced Virgo without a long phase of tests and prototypes. The baking system is already implemented in Virgo, tested and working, hence it will not be discussed here. The expected performance of the cryolinks, after bake-out of the ITF arms, is shown in Table 1, where the contributions of the different gases are reported separately.

Table 1.1. *Proposed goal for phase noise (baked ITF arms) in the 200 - 400 Hz frequency band.*

Gas species	Pressure [mbar]	Noise [$\sqrt{\text{Hz}}$]
Hydrogen	1×10^{-9}	9.7×10^{-26}
Water	1.5×10^{-10}	2.5×10^{-25}
Air	5×10^{-10}	5.6×10^{-25}
Hydrocarbons	1×10^{-13}	2.9×10^{-26}
Total	1.7×10^{-9}	6.2×10^{-25}

The noise is caused by phase fluctuations due to scattering of the laser beam (YAG with a wavelength of 1.064 μm) from background gas. Assuming a gaussian beam and weak scattering the power spectral density of the optical pathlength is given by [1, 2]

$$S_L(f) = \frac{4\rho\,(2\pi\alpha)^2}{v_0} \int_0^{L_0} \frac{1}{w(z)} e^{-2\pi f w(z)/v_0} dz, \qquad (1)$$

where the integral is over the beam axis and cavity length L_0. Note that the finesse $\mathcal{F}$ is not contained in this expression, since the photons during their lifetime probe the same scattering centers in the cavity and hence the phase noise from different bounces adds coherently. The parameters are defined as follows:

$w(z)$ Beam radius. For a gaussian beam it is given by

$$w(z) = w_0\sqrt{1 + \frac{(z - z_0)^2}{z_R^2}}, \qquad (2)$$

where w_0 is the waist, z_R the Rayleigh range (213 m for AdV) and z_0 the waist position along the axis. For AdV the beam waist will be 8.5 mm and is located at 1385 m from the input mirror. The beam radius on the input mirror (radius of curvature $R_{\mathrm{IM}} = 1416$ m) will be 56 mm and on the output mirror ($R_{\mathrm{EM}} = 1646$ m) is 65 mm.

v_0 Most probable speed of the molecular species. It is given by

$$v_0 = \sqrt{\frac{2k_BT}{m}}, \tag{3}$$

where m is the molecular mass. The Boltzmann constant is represented by k_B and the temperature by T. For room temperature (300 K) we find $v_{\mathrm{N_2}} = 422$ m/s and $v_{\mathrm{H_2O}} = 526$ m/s.

α Molecular polarizability of the gas. The polarizability for nitrogen is $\alpha(\mathrm{N_2}) = 1.6 \times 10^{-24}$ cm^3. Note that the Lorenz-Lorentz relation

$$\frac{4\pi}{3}\sum_A \rho_A\alpha_A = \frac{n^2-1}{n^2+2}, \tag{4}$$

connects the refraction index and density fluctuations via

$$\frac{4\pi}{3}\sum_A \delta\rho_A\alpha_A = \frac{6\overline{n}}{(\overline{n}^2+2)^2}\delta n \approx \frac{2}{3}\delta n. \tag{5}$$

The molecular polarizability is best derived [1] from measurements of the refractive index of the gas, n, at wavelength $\lambda = 1064$ nm,

$$\alpha(\lambda) = \frac{n(\lambda)-1}{2\pi\rho_{\#}}, \tag{6}$$

where $\rho_{\#} = \frac{N_AP}{RT}$ is the number density of the gas (# molecules/m^3) with $R = 0.06236$ m^3/(Torr mol K) and $N_A = 6.022 \times 10^{23}$ #/mol. At 1 atm and room temperature $\rho_{\#} \approx 2.4 \times 10^{19}$/cm^3. The molar refractivity measures the polarizability per mol and is given by $A = \frac{4\pi}{3}N_A\alpha$ in cgs units. The molar refractivity remains remarkably constant as the density or pressure is varied, even when there is a change of state. It holds as well for mixtures, when the separate values of A are weighted by the relative number of molecules. For water it amounts to $A_{\mathrm{H_2O}} = 3.71$, while for nitrogen we have $A_{\mathrm{N_2}} = 4.37$. The atomic refractivity of oxygen is 2.01, hydrogen 1.02, carbon 2.11, sulphur 8.23 and chlorine 5.72, so the molar refractivities of many organic compounds can be estimated.

LIGO has experimentally validated Eq. (1) (see ref. [2]). It is based on the following assumptions:

- collisions between molecules are not important (the mean free path for water molecules amounts to $\lambda = xxx$ at a pressure of 10^{-7} mbar);
- a molecule emerges after a collision with the beam pipe with a Boltzmann distribution for its velocity;
- only forward scattering of light is taken into account.

The transversal motion of molecules through the gaussian beam profile leads to a pulse-like dependence of the phase noise. The exponent in Eq. (1) corresponds to the Fourier transform of this pulse shape. The exponential cut in the integral is effective for frequencies greater than the inverse of the typical time needed by a molecule of a given species to travel the distance $2\pi w(z)$. The cut-off frequency is typically in the kHz region (see the curve for the contribution from excess gas in Fig. 2).

The ITF measures the difference in lengths of the two arms and this will have amplitude spectral function $\Delta\tilde{L}(f) \equiv \sqrt{S_{\Delta L(f)}} = \sqrt{2S_L(f)}$. Note that the amplitude spectral density of the pathlength is given by

$$S_L(f) = \left(\frac{dS_L(f)}{d\phi}\right) S_\phi(f), \tag{7}$$

where $S_\phi(f)$ is the phase noise. The phase noise $\Delta\phi$ is related to the length noise by $\Delta l = \frac{\lambda}{2\pi}\Delta\phi$.

For a realistic situation, a sum needs to be taken over all the molecular species present inside the beam pipe. Pressure gradients along the beam pipe are small, but it is possible to take them explicitely into account through integration. Also the beam waist changes in the cavity (see Fig. 3) and its variation should be included in the integration. The diameters of the beam at the

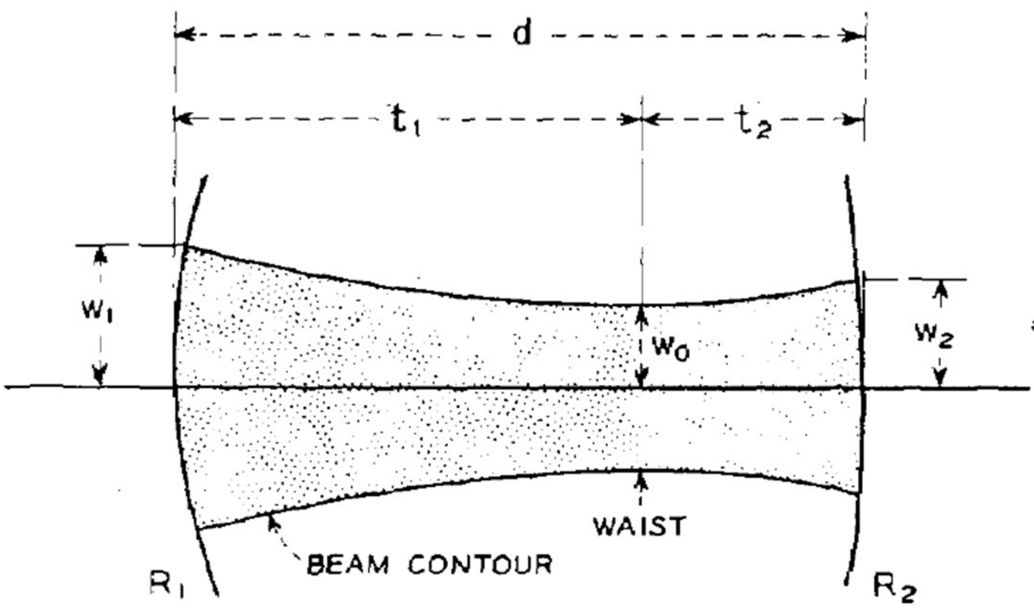

Figure 3: Mode parameters of interest for a resonator with mirrors of unequal curvature (from Ref. [3]).

mirrors of a stable resonator, $2w_1$ and $2w_2$, are given by

$$\begin{aligned} w_1^4 &= \left(\frac{\lambda R_1}{\pi}\right)^2 \frac{R_2-d}{R_1-d}\frac{d}{R_1+R_2-d}, \\ w_2^4 &= \left(\frac{\lambda R_2}{\pi}\right)^2 \frac{R_1-d}{R_2-d}\frac{d}{R_1+R_2-d}, \end{aligned} \tag{8}$$

where the radii of curvature of the mirrors are denoted R_1 and R_2. The diameter of the beam waist $2w_0$ is given by

$$w_0^4 = \left(\frac{\lambda}{\pi}\right)^4 \frac{d(R_1-d)(R_2-d)(R_1+R_2-d)}{(R_1+R_2-2d)^2}. \tag{9}$$

The distances t_1 and t_2 between the waist and the mirrors, measured positive as shown in Fig. 3, are

$$t_1 = \frac{d(R_2-d)}{R_1+R_2-2d}, \quad \text{and} \quad t_2 = \frac{d(R_1-d)}{R_1+R_2-2d}. \tag{10}$$

The elements of the $ABCD$ matrix (see Ref. [3]) of this system can be used to calculate the mode parameters of the resonator. This yields for the corresponding beam radius w

$$w^2 = \left(\frac{2\lambda B}{\pi}\right) / \sqrt{4 - (A + D)^2}. \tag{11}$$

If z measures the distance along the optical axis from the position of the beam waist w_0, the Gaussian beam radius inside the cavity reads

$$w(z) = w_0 \sqrt{1 + \left(\frac{z}{z_R}\right)^2}, \tag{12}$$

with Rayleigh range $z_R = \frac{\pi w_0^2}{\lambda}$. Fig. 4 shows the beam radius distribution for the Advanced Virgo baseline design. The choice of beam waist affects the phase noise contribution. The noise

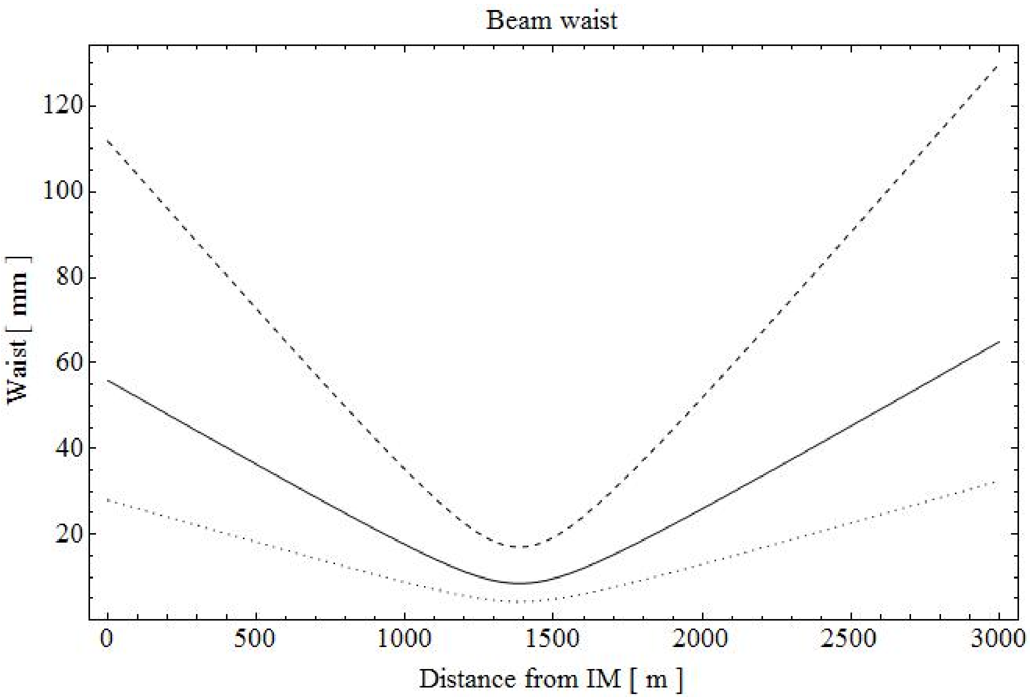

Figure 4: Beam radius distribution for Advanced Virgo (solid curve). The dashed (dotted) curve shows the distribution for a factor two larger (smaller) beam waist.

amplitude roughly increases as the square root of the waist. However, also the shape of the frequency spectrum is affected (a smaller beam radius leads to a harder noise spectrum).

Fig. 5 shows noise strain spectral amplitude densities due to the presence of nitrogen, water vapor, hydrogen and hydrocarbons in the interferometer arms. The figure reveales a weak dependence on the beam waist. A smaller beam size leads to a larger amplitude (the dependence roughly scales with the inverse square root of the waist). Furthermore, it is seen that a smaller waist leads to larger amplitudes at high frequencies. In order not to limit the strain sensitivity of Advanced Virgo, the partial pressure due to water vapor should be smaller than about $P_{H_2O} \leq 10^{-9}$ mbar.

The previous expressions for the noise power spectrum can be used to determine the highest partial pressure that is compatible, for a given species, with a desired noise level. If we choose a

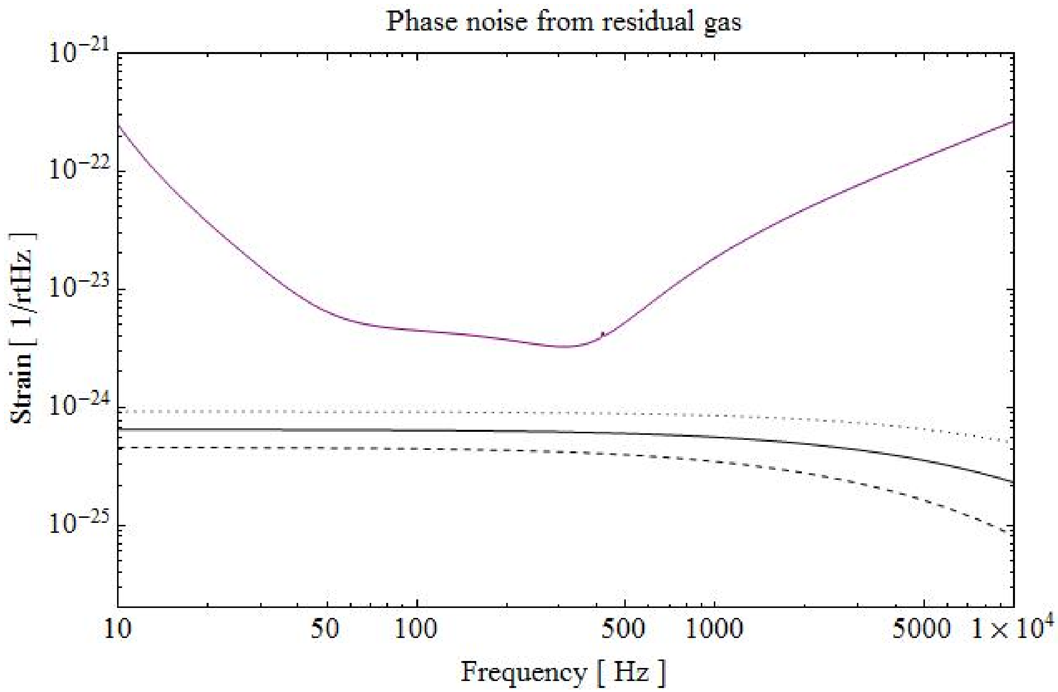

Figure 5: Phase noise due to scattering of the laser beam from the residual gas. The different gas species have partial pressures given in Table 1.1. The purple curve represents the design sensitivity for Advanced Virgo.

particular species (*e.g.* water) as a reference, we obtain the simple expression

$$P_A = P_{\mathrm{H_2O}} \left(\frac{\alpha_{\mathrm{H_2O}}}{\alpha_A}\right)^2 \sqrt{\frac{m_{\mathrm{H_2O}}}{m_A}}, \tag{13}$$

which can be used to obtain estimates for the low frequency region.

2 Technical description

2.1 Task: Mechanical design

There is sufficient space to install cryolinks in between the towers and the existing DN1000 valves. The distance between the face of the mirror and the centerline of the valve is 5400 mm. Fig. 6 shows that the cryostat can be separated from the tower with a DN630 valve (650 mm inner diameter). The vacuum vessels of the cryolinks will have different lengths (links at the end-towers are 6000 mm long, and at the input-towers 5400 mm). Adapter pieces of 100 (600) mm length are used to connect the cryostat to the input (end) tower. We strive towards producing four identical cold vessels in the cryolinks. However, since the optical design is not completed at this point, it may be that the dimensions of the protype will slighty deviate from that of the other links. Since we intend to install the prototype as an actual link, probably near the end-mirrors, a special adapter piece may be needed. Connections with 200 mm diameter for the titanium sublimations pumps are included. The cryolinks have a cold surface with a length of 2023 mm

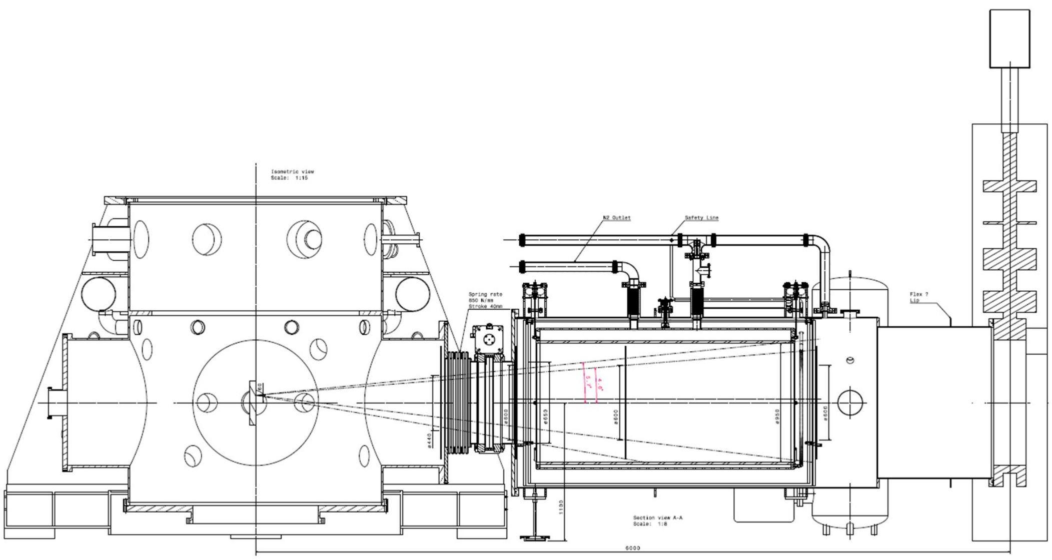

Figure 6: Installation of cryolinks at the west input tower.

and an inner diameter of 950 mm. Baffles will be bolted to the stainless steel vacuum vessel via support bars. These baffles with 600 mm inner diameter will be used to screen the optical path between mirror and cold surface (see Fig. 7). These baffles are connected with spring lips that maybe welded to the inner cylinder. The cryolink at the input mirror has a length of 3212 mm and at the end mirror 3812 mm. The vacuum vessel has an outer diameter of 1350 mm (not including the reinforcement ribs). The outer vacuum vessel will be constructed from stainless steel 304L[1]. Reinforcement ribs are welded to the outside of the vessel to avoid buckling of the structure. Heliconflex seals are used to connect the cryolink to both valves (also the side flange of the cryolink is sealed with heliconflex). The connection to the bellows are made with dry Viton rings.

The vessel is equipped with various pump-out and service ports. An isometric view is given in Fig. 8. A 100 mm diameter top flange provides connection to a turbo-molecular pump station. A section view is given in Fig. 9, while a topview is given in Fig. 10

Fig. 7 shows that stainless steel hydro-formed bellows are foreseen as a connecting piece between

[1]The use of stainless steel 316L has been discussed, but provides no advantage at liquid nitrogen temperature.

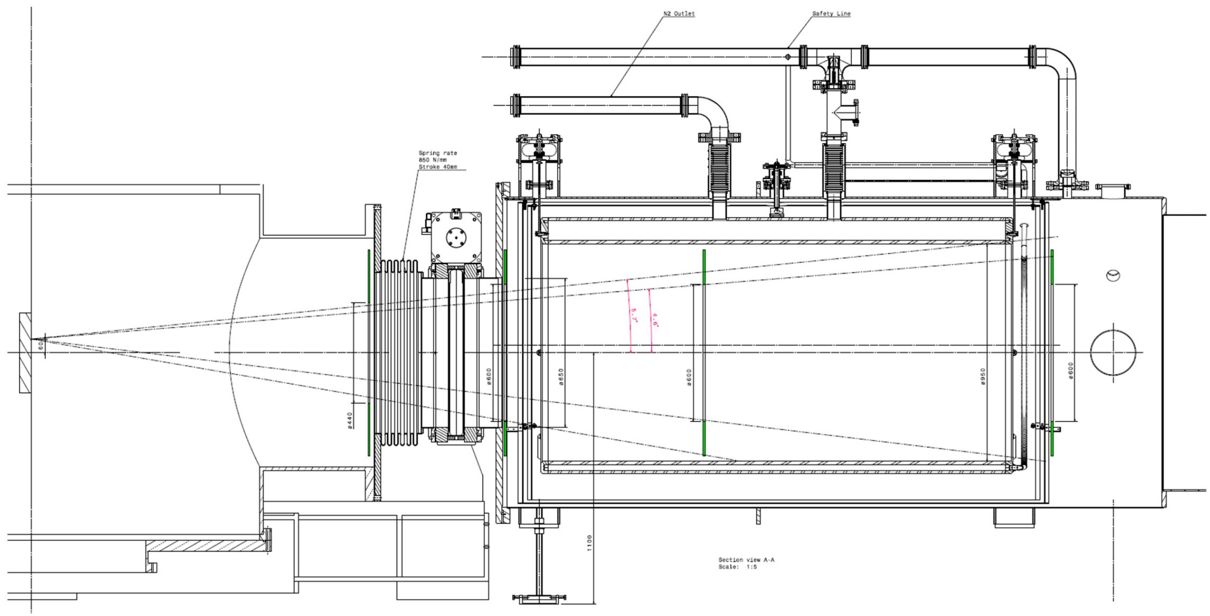

Figure 7: Cryolink with internal baffles for shielding the mirror from direct view of the cold surface. Internal baffles are shown as example of feasibility. The optimal solution for the diffused light mitigation is to be studied, see Task 2.4.

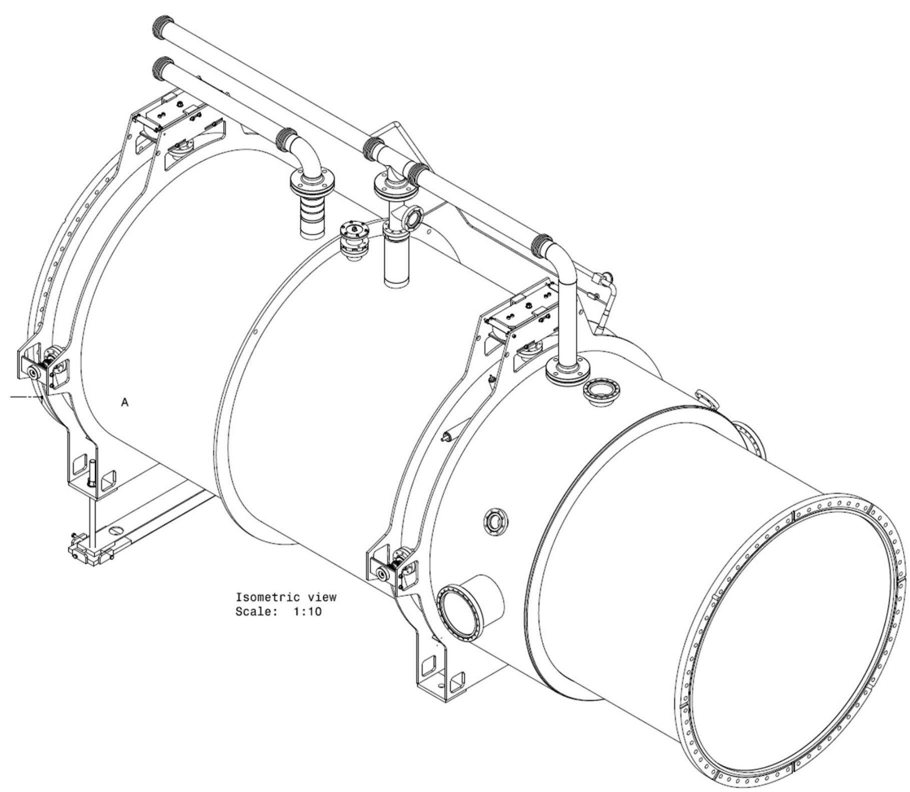

Figure 8: Isometric view of a cryolink for Advanced Virgo. The reinforcement rings and the suspension system is visible. At the top the large nitrogen exhaust lines can be seen.

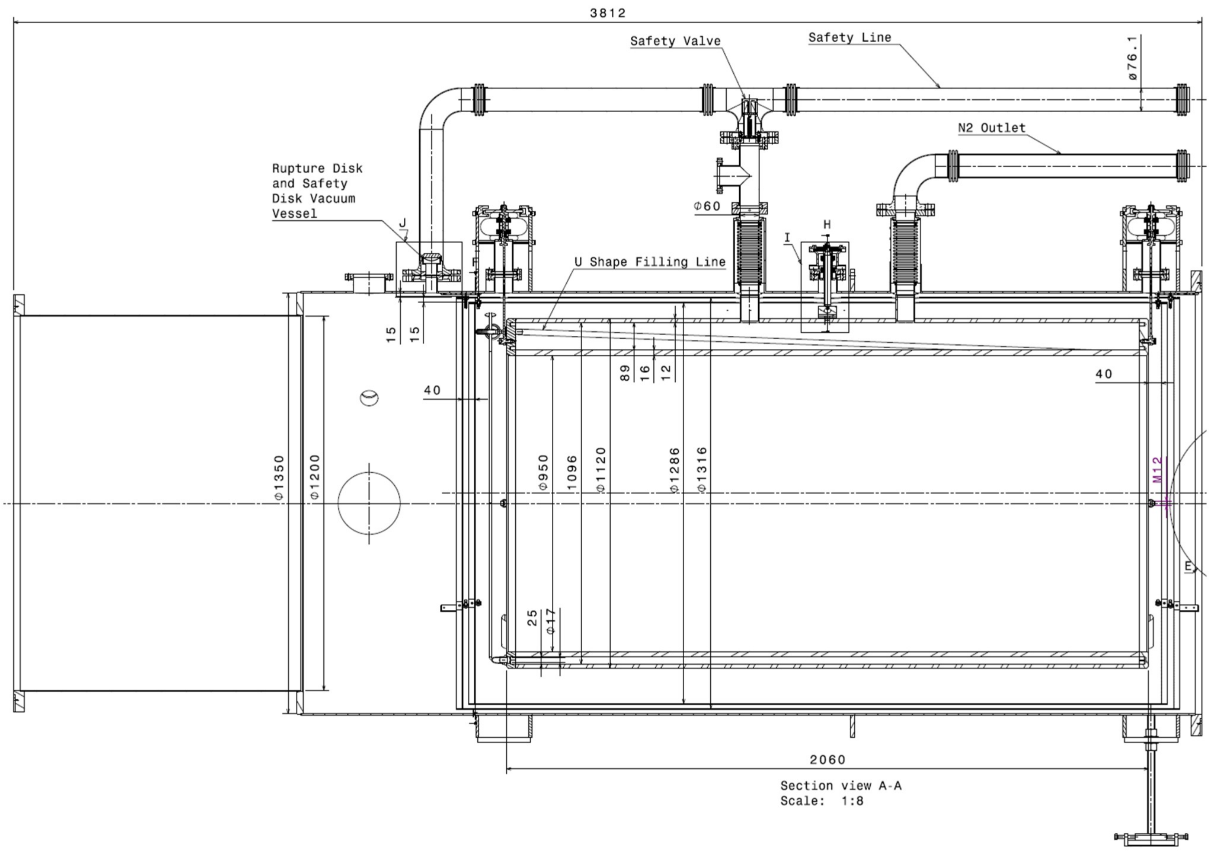

Figure 9: Section view of a cryolink for Advanced Virgo. Aluminum-stainless steel transition material is used to connect the inner vessel to the outside world.

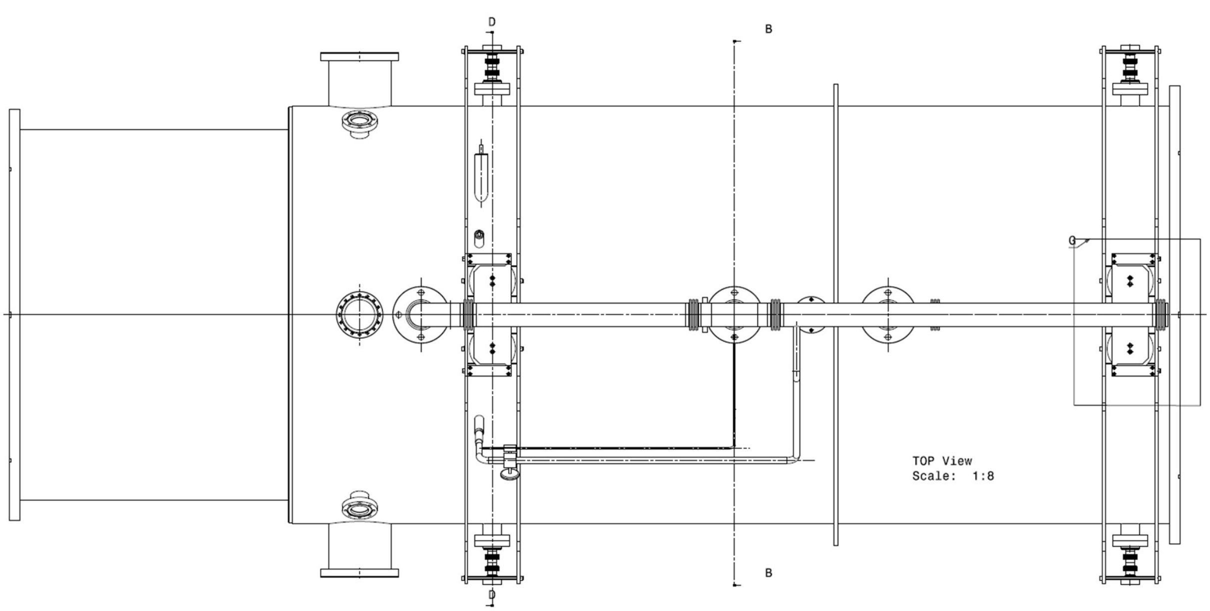

Figure 10: Top view of a cryolink for Advanced Virgo.

the trap and the tower. These bellows have a 700 mm inner diameter and can accommodate expansion of the structure. This is needed during installation of the links, while also thermal expansion during bake-out must be accommodated. Its size has been verified to be compliant with optical constraints. The particular construction has been chosen in order to minimize the atmospheric load on the structures when the tower is vented. Moreover, the present design facilitaties the assembly of the link. Fig. 11 shows a safety detail of the construction of the cryolink. Since the inner cold surface will move due to thermal expansion (about 4 mm/m) with

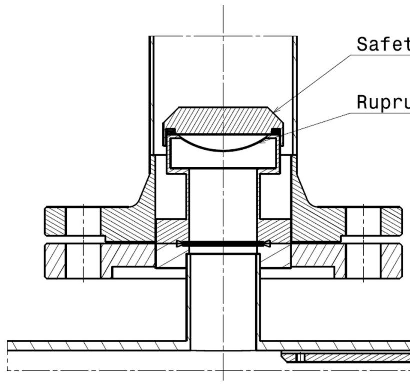

Figure 11: Construction detail of the cryolink: a rupture disk in combination with a safety disk on an O ring are employed as safety device.

respect to the outer vacuum vessel, the suspension system needs to accommodate this. This system also acts as a heat bridge that minimizes thermal losses due to heat conduction. Proper modifications shall be performed on the tower ovens to allow the installation of the cryotraps.

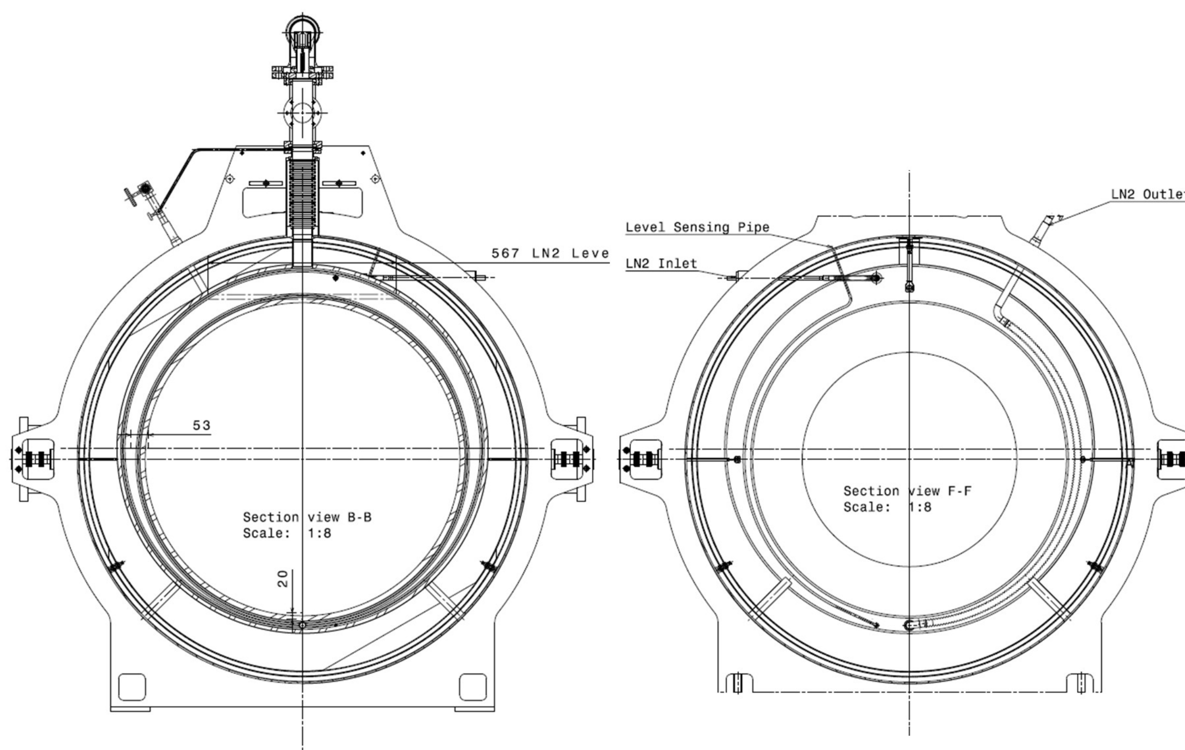

Figure 12: Cross section of the cryolink. The outer vessel of the cold link is placed off-axis with respect to the vacuum vessel. The inner vessel of the cold link is placed on-axis.

The cold part of the cryolink will be constructed from aluminum and the inner surface of the link is cooled with liquid nitrogen. The volume of the bath is about 300 l. This bath is thermally shielded from the outer surface of the vessel by using a double aluminum radiation shield to minimize boiling and LN2 consumption.

Fig. 12 shows a cross section of the cryolink. It is seen that the inner cold link vessel is placed asymmetrically off-axis by 32 mm. In this way the LN2 surface is maximized to 550 mm over the full length of 2000 mm.

The inner link is suspended from the vessel by using two double air springs, in combination with longitudinal and transverse suspension systems (see Task 2.1.1). The design is shown in Fig. 13.

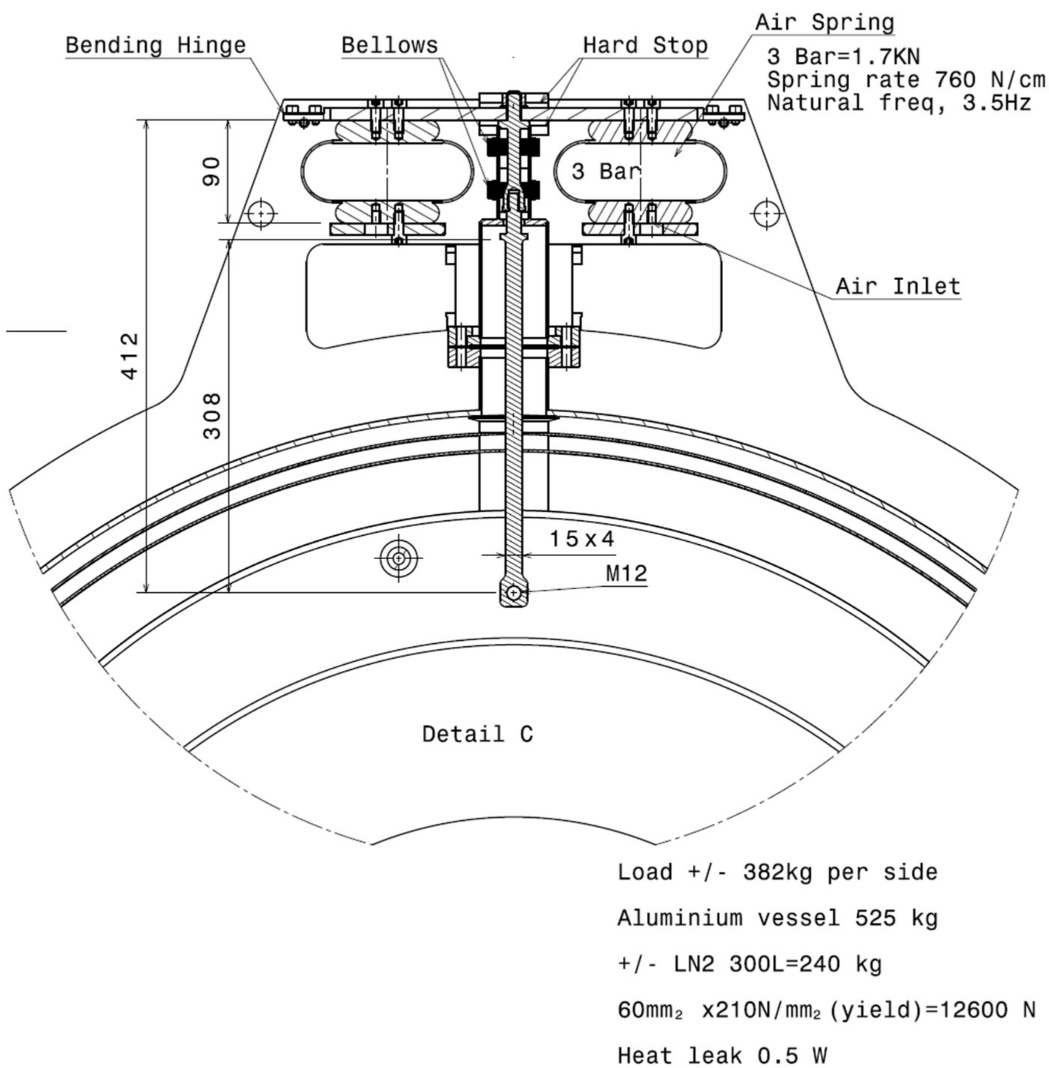

Figure 13: The cold vessel of the cryolink is suspended with air springs in order to isolate Advanced Virgo from possible bubbling noise in the LN2.

The LN2 inlet will be designed such that LN2 will flow smoothly into the bath (laminar flow is ensured by the design), in this manner minimizing any induced noise from bubbling. The liquid nitrogen level in the bath can be controlled to within ± 10 mm. Note that the bath has a sizable width of about 550 mm. Again this guarantees that bubbles have a large escape path to the surface over the entire 2000 mm length of the cryotrap. A separate LN2 inlet is provided in order to admit hot nitrogen gas in case rapid heat-up of the structure is needed. The cryotrap can be operated for more than one year between regenerations, assuming a load of 10^{-4} mbar l/s from the mirror vessel (see Task 2.2.1). During this time a nitrogen layer of about 1 micron will be deposited on the inner surface. This causes the initial emissivity of about 0.1 to increase to 0.2. This relative low value for the emissivity leads to an average heat load of about 250 W, and results in an estimated LN2 consumption of about 5.6 LN2 per hour[2]. This corresponds with an estimated gas production of 1 l/s, assuming 80 K surrounding temperature in the vessel.

Some parts of the cryolinks (such as new parts of stainless steel exposed to vacuum and operating at room temperature) have to be 'fired' (*i.e.* heated at 400° C in air or argon for about one week. This treatment will be normally done in the factory during the production phase, unless we will consider to perform it on-site (EGO or Nikhef) in order to save money.

2.1.1 Sub-task: Bubble noise

Two-phase (liquid-gas) nitrogen flow modeling must be performed. We will focus on the study of the liquid - vapor flow inside the cryolink. The design will be optimized with respect to acoustic and mechanical noise due to bubbles. The work will be carried out in collaboration with scientists from EGO and the University of Pisa [4]. The noise spectrum is determined partly by the diameter of the bubble and the frequency of nucleation. These parameters have been studied by several researchers. In 1970 Bewilogua *et al.* [5] presented the bubble frequency as function of the diameter for several cryogenics liquid. They found for the nitrogen fluid the bubble frequency f and the bubble diameter D are correlated by the equation:

$$f \cdot D^2 = 7.6 \text{ mm}^2/\text{s}. \tag{14}$$

Fuchino *et al.* in 1996 [6] found that the correlation proposed in Eq. (14) is weakly influenced by the roughness of the surface and heating power in the case of boiling liquid nitrogen.

We will design and construct a test system consisting of a LN2 vessel enclosed in a 80 K environment (a dewar). The system will feature a 1 m long vertical surface that contains a distributed heating element. Sensors will be used to determine whether heat transfer takes places through convection cooling or whether bubbles are produced (microphone, visual inspection through fibers). Different surfaces will be used (*e.g.* aluminum, various surfaces finish: blank and silvered surfaces, vary surface roughness).

2.1.2 Sub-task: Suspension system for vibration isolation

The cryolink and baffle system will experience displacement noise from seismic motion of the floor and possibly bubble noise. We propose to incorporate a well-damped suspension system based on air-springs to isolate the system from bubble noise produced by the cold LN2 part. The LN2 vessel will be connected to the vacuum pipe via this system. The resonance frequency will be about 3 - 4 Hz and the Q-factor about 10 to 20. A well-damped system is needed since there will always be up-conversion from low frequencies (around 0.5 Hz) or modes at low frequencies. High-frequency noise from bubbles may influence the sensitivity of Advanced Virgo through back-scattering. The cold trap will be isolated from the ground through an air-spring based suspension system. The various elements of the suspension system are shown in Fig. 14. The silicon rubber spring for horizontal positioning allows movement from thermal contraction/expansion and specifically retricts motion in the xy-plane (transverse). The air-spring system for vertical isolation needs to allow vertical motion *e.g.* during bake-out. The flexible hinges located at the top provide

[2]The heat of evaporation of LN2 amounts to 199 kJ/kg. The density is 0.8 kg/l.

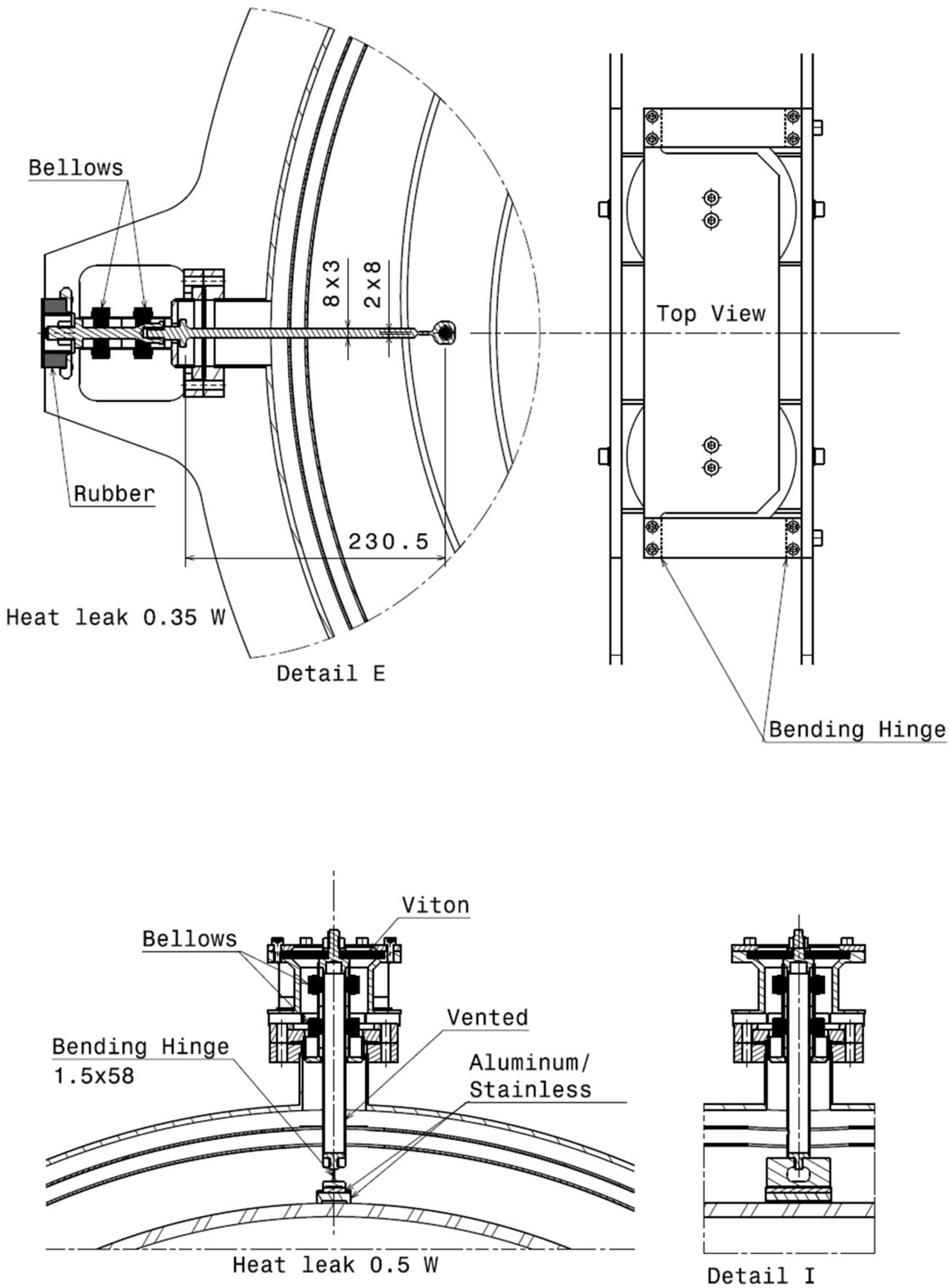

Figure 14: Suspension system for the cryolink. Left: silicon rubber spring for horizontal positioning; middle: air-spring system for vertical isolation; right: top view of the flexible hinges. See Fig. 13 for a cross section of the central air spring suspension system.

guidance for vertical displacement (but not horizontal) of the top of the air springs. It has to be investigated to what extend the bellows by-pass the suspension isolation.

A preliminary simulation of noise from back-scattered light from the cryolinks of Advanced Virgo has been carried out by Fiori [10]. It is based on the noise model described in Ref. [9] and realistic seismic noise (see Fig. 15) obtained from the measured horizontal displacement of the existing Virgo cryogenic trap. Fig. 15 shows the following characteristic noise features

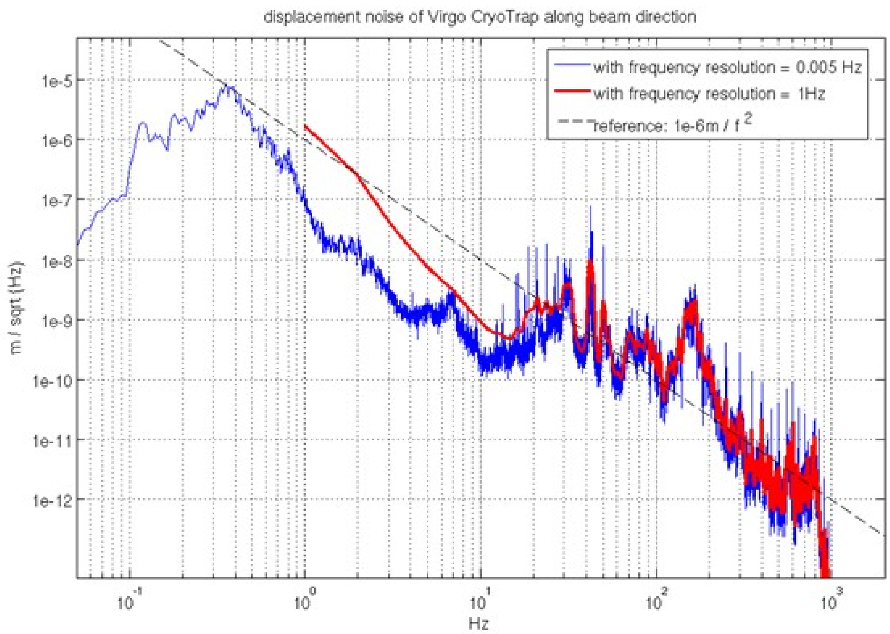

Figure 15: Vibration noise along the beam axis of the existing Virgo cryotrap. The spectrum is measured with a frequency resolution of 1 Hz (the red curve shows the rms value) and with a frequency resolution of 0.005 Hz (blue curve) which is resolving all pseudo-monochromatic vibrations produced by mechanical rotating devices (*e.g.* fans, engines) located in the CB hall. The dashed line shows the reference noise spectrum of $10^{-6}/f^2$ m/$\sqrt{\text{Hz}}$. From Ref. [10].

- A large bump at 0.4 Hz which is associated with sea activity, and in worst conditions (a few % of the time) can reach amplitudes of about 10 μm.
- Several narrow peaks above 10 Hz, which originate from rotating devices in the experimental hall (*e.g.* cooling fans, engines). These peaks have a quality factor Q which is measured to never exceed a value of 2000. The narrowest peaks (in the range from 10 to 50 Hz) have a measured width of 0.01 Hz.
- The noise around 50 - 150 Hz is enhanced (see Virgo's eLogs 24753 and 23722) by about 5 times by the action of LN2 bubbles after refills operations. The excited peaks probably correspond with mechanical resonances of the existing Virgo cryolink. Such resonances should be avoided in the AdV cryolinks.

The scattered light can be estimated by considering an optical path where photons undergo a first scattering event at the mirror surface towards the exposed cryolink walls, then a second pure back-scattering event from the cryolink walls back to the mirror, and a final scattering by the mirror into the ITF beam solid angle. The resulting scattered light noise is given by (see Ref. [9])

$$h_{\rm sln}(t) = \kappa \sin(\phi(t) + \Phi_0), \tag{15}$$

with $\phi(t) = \frac{4\pi}{\lambda} z(t)$ the phase delay of the scattered field with respect to the main beam, $z(t)$ the displacement of the cryolink walls along the beam direction. The angle Φ_0 is the static phase difference between the scattered field and the main field. The coupling factor κ depends on geometrical parameters and scattering properties of the mirror and trap walls. It has been estimated at $\kappa = 2 \times 10^{-25}$ m/$\sqrt{\rm Hz}$ [12].

When the displacement noise of the cryolinks is small, $z(t) \ll \frac{\lambda}{4\pi} \approx 10^{-7}$ m, then Eq. (15) can be approximated by

$$h_{\rm sln}(t) = \kappa \frac{1}{\sqrt{2}} \frac{4\pi}{\lambda} z(t), \tag{16}$$

and Fig. 15 shows that the linear case condition ($z(t) < 10^{-8}$ m) holds for most of of the vibration noise spectrum (exceptions are the microseism and the cooling fans that around 50 Hz). Note

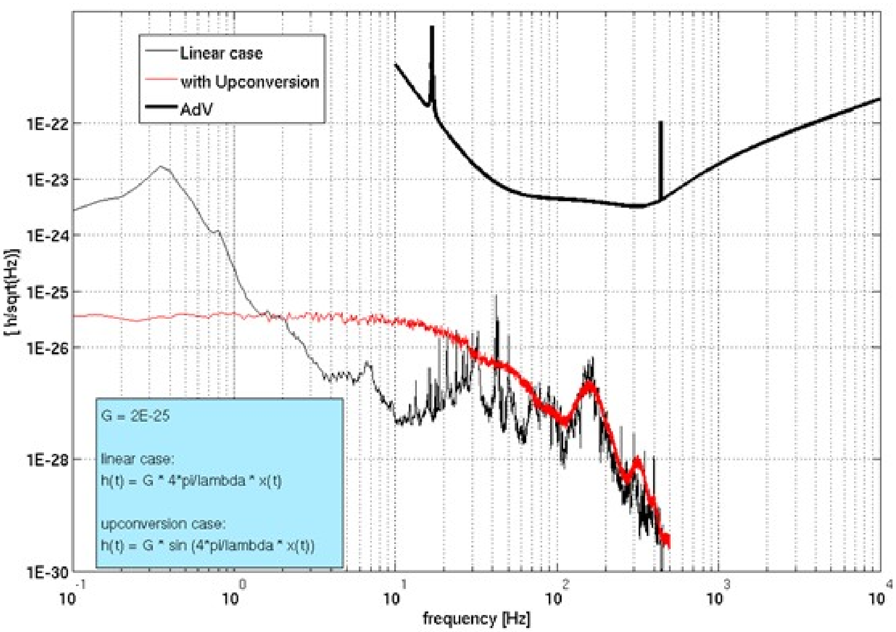

Figure 16: Projected noise from AdV cryotrap for $\kappa = 2 \times 10^{-25}$ m/$\sqrt{\rm Hz}$ and assuming that the vibration noise is the same as that of the existing Virgo cryotrap. The predicted noise (red curve) is compared to the prediction from the linear approximation (black curve), and to the AdV design sensitivity. From Ref. [10].

that in the linear case the scattered field vector undergoes small angular displacements around its position (Φ_0) and the averaging of the slow drift of the static phase leads to the term $1/\sqrt{2}$. The results for the linear case are shown in Fig. 16.

For large vibration noise ($z(t) > 10^{-8}$ m) the non-linear term in Eq. (15) cannot be neglected. The behavior of spectral noise in the non-linear case has been described in Refs. [13, 14, 15] and can be understood as follows. Each time $z(t)$ changes by $\lambda/2$ the phase angle $\phi(t)$ varies by 2π. Thus the scattered field vector (see Fig. 17) completes one full turn and $h_{sln}(t)$ completes one

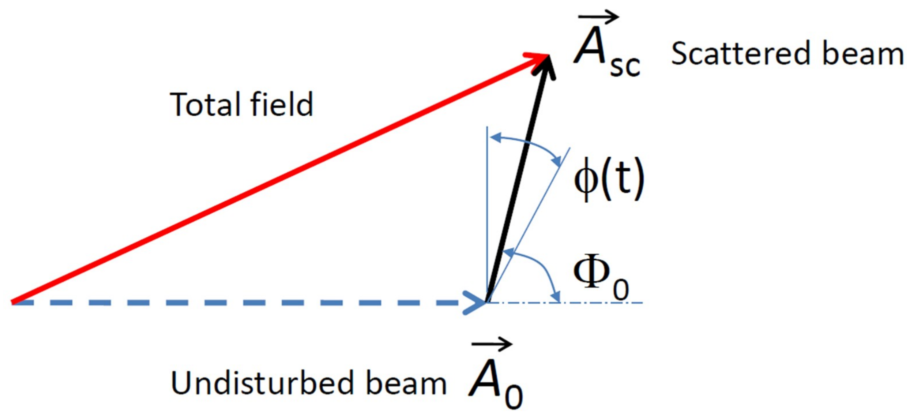

Figure 17: Schematic representation of the scattered field A_{sc}, its phase Φ_0 with respect to the ITF beam A_0, and its changing phase angle $\phi(t)$. From Ref. [10].

oscillation. The number of such oscillations per second, *i.e.* the frequency of the strain noise, is

$$f_{\rm sln} = \frac{2}{\lambda}\dot{z}(t), \tag{17}$$

where, $\dot{z}(t)$ is the velocity of the walls of the cryolink, the first order time-derivative of $z(t)$. In the special case (which is often valid) that the wall-vibration of the cryolink is monochromatic, $z(t) = A_0 \sin(2\pi f_0)$, Eq. (17) gives the maximum frequency of the h_{sln} spectral noise:

$$f_{\rm max} = \frac{4\pi}{\lambda}A_0 f_0. \tag{18}$$

Qualitatively, what happens is that a monochromatic displacement noise (A_0, f_0) produces a shoulder in the $h_{\rm sln}$ spectrum which extends up to $f_{\rm max} > f_0$ (so-called 'up-conversion'), and has an rms value $\sigma(h_{\rm sln}) = \kappa\sqrt{\frac{2}{f_{\rm max}}}$ (see Ref. [11]).

Fig. 16 compares the predicted noise of backscattering, using both the non-linear (red curve) and linear (black curve) approximation for intense micro-seismic activity. The effect of up-conversion of the micro-seismic peak ($A_0 = 8 \times 10^{-6}$ m) is evident: the shoulder extends up to $f_{\rm max} \approx 35$ Hz, and has amplitude $\sigma(h_{\rm sln}) \approx 4 \times 10^{-26}$ m$/\sqrt{\rm Hz}$ as predicted by the above equations.

Fiori [10] deduces two simple rules for up-conversion noise in the detection band ($f_{\rm max} > 10$ Hz):

1. as long as κ guarantees a safe limit for the linear approximation, the up-conversion noise in the AdV detection bandwidth is limited as well. Its spectral amplitude is $\sigma((h_{\rm sln}) = \kappa\sqrt{\frac{2}{f_{\rm max}}} < \kappa$ (if $f_{\rm max} > 10$);
2. it seems a good safety rule to avoid the onset of up-conversion noise inside the ITF detection band ($f_{\rm max} > 10$ Hz) by
   (a) avoiding wall vibrations of the cryolink with frequencies $f > 10$ Hz and amplitudes $z > 10^{-8}$ m;
   (b) avoiding walls vibrations with frequencies $f < 10$ Hz and amplitudes z, such that $f \times z > \frac{\lambda}{4\pi} \times 10$, or velocities $v > \frac{\lambda}{2} \times 10$, *i.e* velocities greater than 5×10^{-6} m/s. This means that a possible resonance mode of the seismic isolation system of the cryolink, which for example is at $f = 5$ Hz should have amplitude $z < 10^{-7}$ m.

We propose to employ air suspensions from ContiTech AG. These air isolators are mounting elements of natural frequencies in the range 3.2 - 3.5 Hz. The spring force is obtained from the compression of the gases they contain. These isolators effectively suppress the transmission of vibration and structure-borne sound to the surroundings. Air isolators also reduce the effects of vibration by isolating sensitive equipment from the source. Damping limits vibration amplitudes to a permissible ratio. Lehr's damping ratio[3] D of standard air springs is 0.03.

The air isolators will be mounted so that the shortest distance between points of support is at least twice the height of the centre of gravity above the plane of support. This minimizes wobble and prevents operational problems. The spring stiffness of an air isolator results from the compression of the air volume it contains. The axial stiffness can be reduced further by using an auxiliary volume. This will be studied on the prototype. Depending on the dimensioning of the connection line between air isolator and auxiliary volume, a non-wearing, non-ageing air suspension system is created. If the connection line has a shut off system, the air spring suspension system can be switched between two vertical natural frequencies.

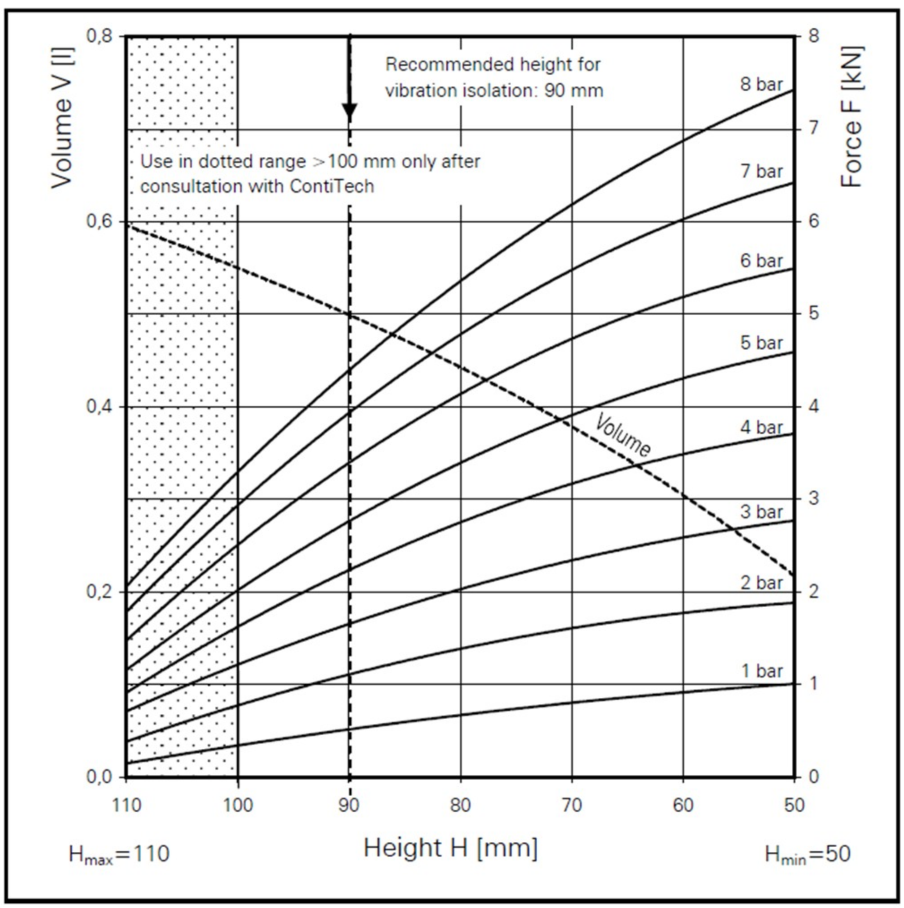

Figure 18: Force height diagram for the FS 40-6 ContiTech single convolution air spring.

[3]The damping factor θ (frequently given as a percentage and previously referred to as Lehr damping factor $D = \theta$) is a measure of the decrease in amplitude of a free decay process. Alternative and equivalent characteristics to describe the damping of a system are

- the loss factor $\eta \approx 0.5\theta$, and
- angular loss ξ (the phase angle between force and deformation, to be determined for $\eta = \tan \xi$).

It generally applies: the larger θ, the smaller are the maximum increase $z_{\max}(t)$ and the isolation effect of the excitation frequencies larger than 1.4 times the resonance frequency.

We intend to employ the ContiTech FS 40-6 air spring. The aluminum vessel has a weight of 525 kg and will be filled with about 240 kg of LN2. This yields a 191 kg load per air spring. The force-height diagram is given in Fig. 18. Each spring needs an 160 mm diameter installation space. The recommended height of the spring is 90 mm (minimum is 70 mm). This height can be achieved with different combinations of applied pneumatic pressure and force load. The pressure should range from 3 to 8 bar (the corresponding force load then ranges from 1.7 to 4.4 kN). Spring rates range from 760 to 1820 N/cm and the natural frequency decreases from 3.5 Hz at 3 bar to 3.2 Hz at 8 bar.

The lateral stiffness of air isolators differs greatly from type to type. In the cryolink construction part of the axial stifness is taken by the hinges. For the individual air isolator types, the following lateral stiffness values - relative to the axial stiffness - can be expected. The specified percentages are for the recommended operating height for vibration isolation.

- Single convolution air isolators 30 to 60%;
- double convolution air isolators 5 to 30%;
- belted air isolator 30 to 50%.

Triple convolution air isolators, rolling lobe air isolators and sleeve type air isolators have no positive lateral stiffness and can only be used for vibration isolation with lateral guidance. Lateral guidance can also be achieved on rolling lobe air isolators and sleeve type air isolators with the use of a restraining cylinder which turns the air isolator into a kind of guided diaphragm. Because of their low natural frequency, both types are excellent vibration isolators. However, we prefer to refrain from lateral guidance systems and propose to use single convolution isolators.

Height regulation can be achieved by supplying the isolators with air in various ways.

- Tank valve: For applications involving a constant load and where small differences in height are permissible, a tank valve can be employed. After the initial inflation, the air pressure or the operating height should be checked regularly and topped up if necessary.
- Pressure regulating system: When several air isolators are linked to a common pressure regulating valve, any lost air is replenished automatically and requires no maintenance. This system makes it possible to level systems with unknown weight distribution. The air isolators are combined into three groups and the pressure control valves are individually set in accordance with the distribution of weight (see Fig. 19). This type of air supply

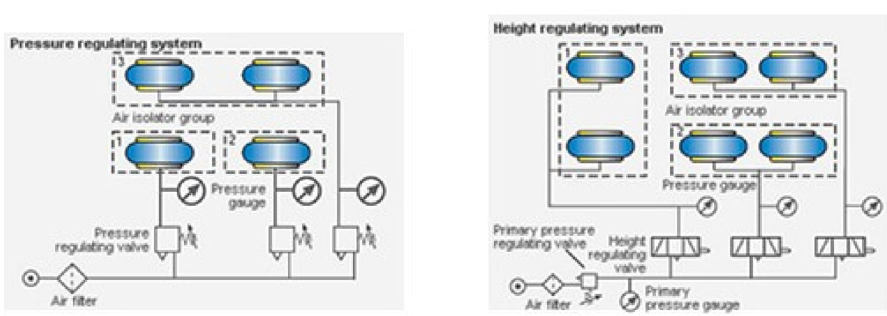

Figure 19: Possible schemes for pressure regulating system and height regulating system.

can be employed only for convolution air springs and sleeve type air isolators of the type SK - so only for air isolators for which the load capacity decreases as the operating height increases.

- Height regulating system: If the height regulation has to be exceptionally accurate or if rolling lobe air springs (types SZ, RZ and LG) are used for vibration isolation, automatic height adjustment valves are required. Height regulation must always be carried out with three control valves so that the level of the machine can be adjusted via three points.

We intend to study the various schemes with the prototype. Attention will be paid to avoid wobbling motion of the LN2.

2.1.3 Action items

1. All dimensions must be fixed as soon as possible to the extent that a prototype can be constructed. To minimize costs, it is foreseen to re-use and install this prototype as an actual link in Advanced Virgo. When major dimensions, such as length and diameter, need modification in the final design, it is expected that the prototype can be installed in a less critical area, *e.g.* near one of the end mirrors.

2. Mechanical design and production of prototype.

   (a) Finite-element analysis of vacuum vessel to determine resonances and constraints for buckling. Determine required wall thickness. This analysis serves as input for the safety certification process. Displacement during evacuation. Stress and displacement of glass baffles. Eigenfrequencies of the vessel. Quantify up-conversion of seismic noise since it is of importance for diffused light scattering from baffles. Determine the transfer function from ground to baffles. Qualification and design of re-inforcement rings (4 weeks).

   (b) Finite-element analysis of inner aluminum vessel and determination of resonances. Study of buckling. Determine eigenfrequencies and damping factor. Prediction of transfer functions from ground to the various baffle locations in order to determine the effect from seismic motion on diffused light noise. Prediction of transfer functions from inner vessel to baffles to determine effect from bubble noise (4 weeks).

   (c) Completion of 3D design (4 weeks).

   (d) Completion of 2D production drawings (6 weeks).

   (e) FEA should be supervised by an FEA expert (Corijn?) (1 day/ 2 weeks).

   (f) Engineering review with cryo-experts (2 weeks).

   (g) Tendering process (avoid this delay for the prototype). Preparation of documentation (*e.g.* vacuum specifications from EGO) (4 weeks).

   (h) Production of prototype (4 months). Quality control of production: vacuum quality (*e.g.* cleaning methods, TIG welds). Assurance of requested production method (1 day/week during prototype production; less frequent during remaining link production when done by the same manfacturer).

   (i) Acceptance test at factory (1 week).

   (j) Transport to and installation at Nikhef site (2 weeks).

   (k) Prototype testing at Nikhef. (16 weeks).

   (l) Design modifications, if any. Tendering process for remaining cryolinks. Preparation of required documentation (4 weeks).

   (m) Cryolink production, quality control, acceptance test at factory (12 months).

   (n) Transport to EGO (2 weeks).

(o) Installation at EGO site (4 months).

(p) Acceptance testing at EGO site (2 weeks).

3. Design of adaptor pieces, flanges for prototype, and bellows. Definition of dimensions (length and diameter) in consultation with Virgo OSD representative (2 weeks).

4. Design of baffle system. Choice of geometery and positions to be made (2 weeks).

5. A detailed description of the assembly procedure should be developed: how and in which order will be the components be mounted. Which gaskets are used where? How is the (TIG) welding accomplished? (1 week).

6. Establish whether firing of cryolink material is necessary (1 week).

7. Design and construction of a test set-up for the suspension system based on air springs. Design and construction of a pressure and height control system. The set-up will employ a 350 kg dummy load (ensure safety measures!). Measure eigenfrequency and study damping (we need a Q factor in the range 10 - 100) (6 weeks).

8. Measure ground motion at position of cryolinks at the EGO site (1 week).

9. Study of two-phase flow and bubble noise. Design and construct a set-up that contains a LN2 volume that is perfectly shielded from thermal radiation (*e.g.* by immersion in a LN2 dewar). Heat can be provided to this liquid with a resistor mounted on a metal plate. Temperature sensors, a camera and microphone will be used to study the boiling behavior. It will be established whether stable conditions for natural convection boiling can be achieved. Variables are the heat density, surface roughness and thickness. Effects of overcooling should be investigated (*e.g.* by pumping on the LN2). We will study the correlation between bubble detachment diameter and nucleation frequency for a given thermal load. In addition, such measurements will be carried out on the cryolink prototype (20 weeks).

10. Prepare the documentation concerning safety issues related to the cryolink (2 weeks).

2.2 Task: Vacuum and cryogenic control systems

The vacuum and cryogenic control system tasks are divided into various subtasks. In the following we will describe some overall simulation results for the vacuum aspects of the cryolinks. In addition, the preliminary design of the vacuum system is presented. For the cryogenic system we give a brief description of the LN2 filling system, and the control and data logging systems. Note that these systems will be provided by our collaborators from INFN Genua and EGO. However, as these systems are used during the prototype tests at Nikhef, we give a brief description here.

2.2.1 Sub-task: Vacuum simulations

Monte Carlo simulations have been carried out by Nikhef and INFN Genua to describe the pressure profile in the Advanced Virgo interferometer. We have considered the typical gas load coming from a mirror tower after 2 days of pumping following an opening intervention. The calculated efficacy of the trap is presented in Fig. 20. The figure shows that with the proposed

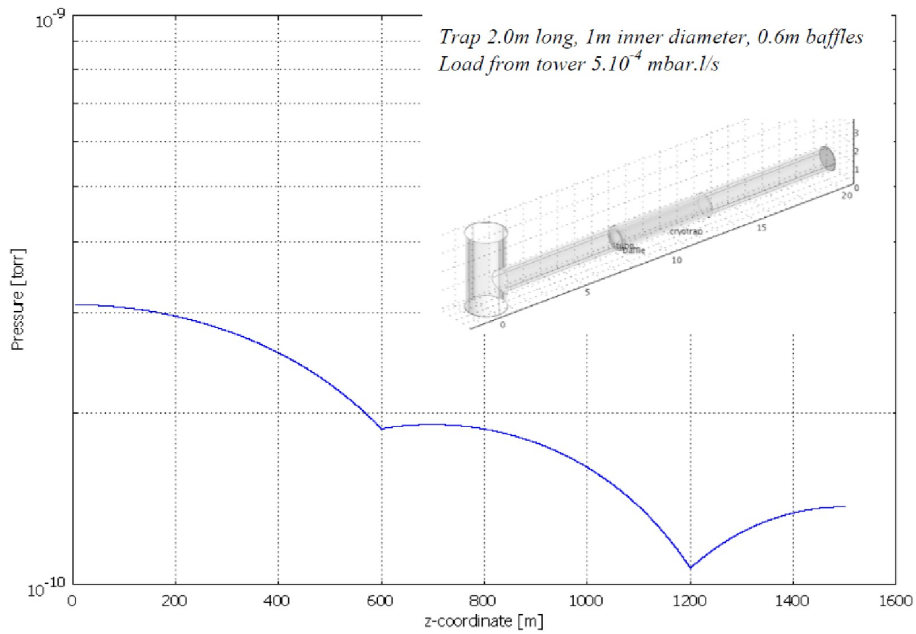

Figure 20: Water pressure profile along the beam tube calculated for selected trap geometry.

cryolink system, the residual pressure in the interferometer arms is less than 10^{-9} mbar, as required by the specifications.

The water 'trapping' performance is given by two effects:

- the majority of water molecules directly hit the inner trap surface, due to the geometrical view factor, and sticking coefficient there: the molecular escape (ballistic) fraction is 2.3 % for a trap with the selected geometry;
- a large part of the transmitted molecules bounces back from tube walls and re-enters inside the trap, being pumped. The pumping speed is proportional to the trap aperture, about 4×10^4 l/s for the selected geometry.

More accurate calculations have been performed both with Monte Carlo methods and with FEA models, to take into account the actual geometry and the presence of optical/thermal baffles near the trap. The most important maintenance intervention with cryolinks is the periodical

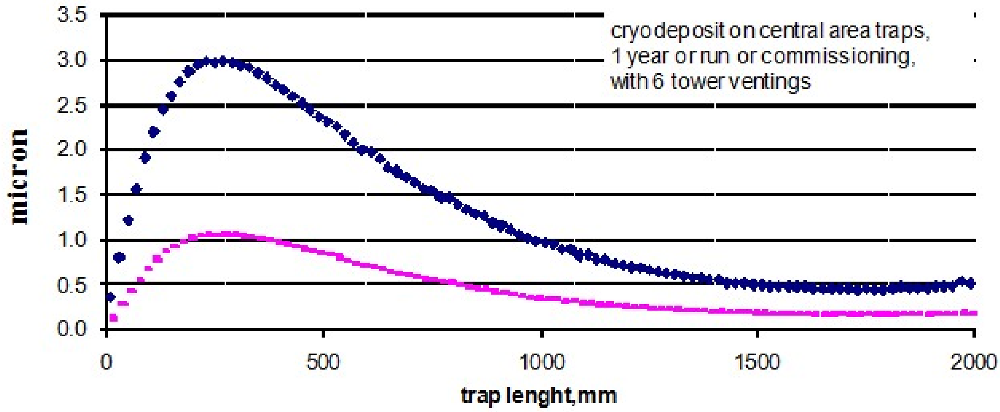

Figure 21: Evaluation of the water deposit that develops along a cryolink after 1 year of service, during run conditions (pink curve, with 2 g of condensed water) or during commissioning (blue curve, with 6 g of water) with frequent ventings (every 2 months, both UHV and bench towers). The evaluation is for a 'central area' trap.

regeneration, which involves a stop of the interferometer for a few days. Regenerations are normally needed to limit the LN2 consumption, since the thickness of the condensed water layer influences the surface emissivity, which is progressively increasing. On the contrary, regenerations are not needed for pumping speed reasons, since the exposed surface temperature will be not significantly increased by the thermal resistance of the thin deposited water (in the order of microns thickness). The relation between emissivity and thickness of the water cryo-deposit is available from experience in the aerospace field [7]. The density of solid water is expected to be near 0.9 g/cm^3 (ice) close the inlet ports of the trap and decreasing versus the interior because the minor angle of incidence (up to 0.6 g/cm^3). An evaluation of the deposited thickness in 1 year of service is presented in Fig. 21. Two conditions are shown: operating in 'commissioning' mode, with frequent interventions inside the towers (every 2 months opening alternatively a bench tower and a UHV tower, for instance), and in a long run, several months after the last venting. The calculation has been done with a Monte Carlo method for a cryolink geometry of 2 m in length, 1 m inner diameter, and 0.6 m diameter baffles at both extremities.

The extra-consumption of LN2 with respect to 'normal running conditions' will be about 50 %, well tolerable by the system hardware. Regeneration of the cryolink will be driven by the extra-cost due to LN2 consumption and the general schedule for AdV activities. In summary, we do not expect to regenerate the cryolinks more than once per year. For comparison, LIGO has not yet regenerated its traps after several years of service.

Nikhef will provide a detailed regeneration procedure.

Nikhef will redo the vacuum simulations for the final prototype design. The results will be compared to measurements on the prototype. The simulation results for LN2 consumption will be compared to the performance of the prototype.

2.2.2 Sub-task: Vacuum system design

Supplementary equipment is needed for each cryolink. A preliminary outline for the vacuum system is given in Fig. 22. Pirani and Penning vacuum gauges will be mounted on the cryolink

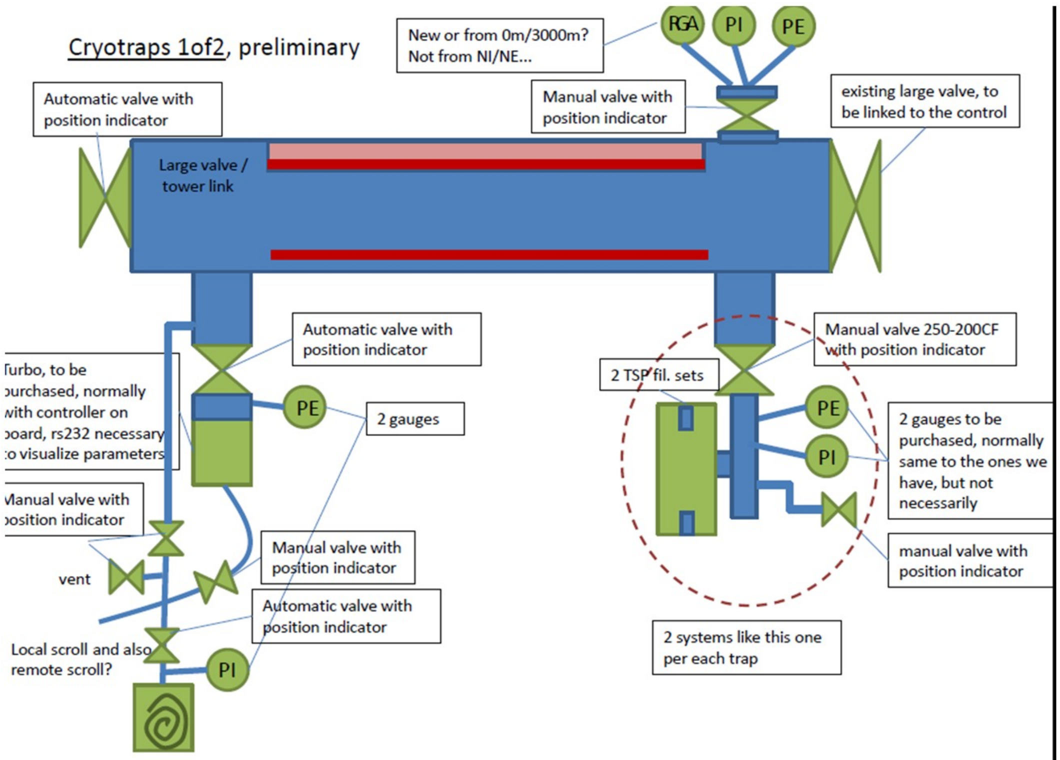

Figure 22: Schetch of the vacuum system for the cryolink. The vacuum system is identical for all links.

volume and connected via a manual valve with position indicator. These gauges will be used to monitor the residual pressure from atmospheric pressures down to 10^{-9} mbar. In addition, a residual gas analyzer will be used for diagnostic purposes.

The system is evacuated by a turbo-molecular drag pump and a dry (scoll) pump [4] which are connected to the cryolink via an automatic 100 mm diameter gate valve with position indicator. The controller of the turbo-molecular pump will have an RS232 connection that is used for visualization of system parameters. The system is equipped with Pirani and Penning gauges (two sets for redundancy). This combination is also needed during regeneration of the cryolink. The scroll pump will be at a remote location. Four small manual valves with position indicators (is this needed?) are used for venting and other logistical tasks.

Two titanium-sublimation pumps are used during normal UHV service. These pumps are connected to the cryolink via a 200 mm diameter gate valve that is manually controlled. The valve is equipped with a position indicator. A double set of Penning and Pirani gauges are mounted on this system. A small valves is mounted for pump-down and venting purposes.

The cryolink is connected to the ITF-arm via a 1000 mm diameter gate valve and to the mirror tower via a 650 mm gate valve. These valves are equipped with position idicators and linked to the control system.

The entire system needs to be available at Nikhef for prototype tests.

Four of these systems need to be developed for all cryolinks and installed at the EGO site. The vacuum system has to be integrated with the Virgo slow-control system.

[4]A scroll pump sufferes from limited compression factor for light gases. A turbo-molecular drag pump allows for higher fore pressure.

2.2.3 Sub-task: Slow control system and data logging

The local control of the cryolinks will be based on PLC-systems that are common at the EGO site (Crouzet control PLCs). The design and realization of the hardware and control software will be done in collaboration with EGO personel.

A PLC-based control system will be used at Nikhef during the prototype tests. The following operational modes can be distinguished: normal operation (bake-out of ITF arms happens only one time), regeneration of cryolinks (at most once per year). Below we present a rough description of the various steps.

Fig. 23 shows the control settings for normal operation.

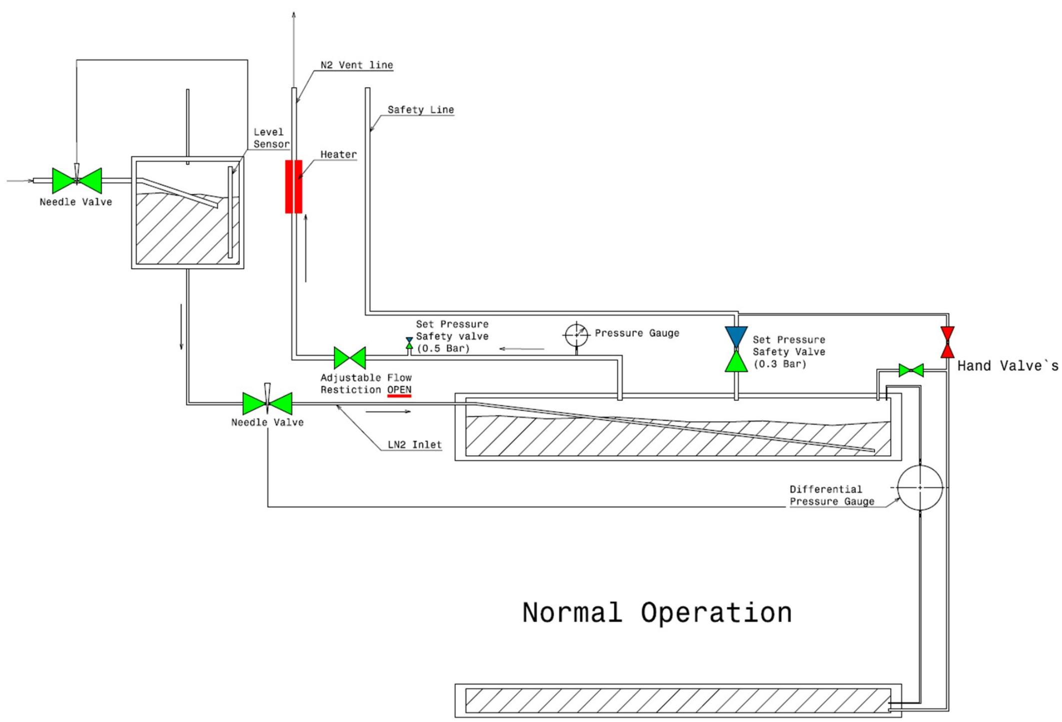

Figure 23: Schematic representation for the control settings of various valves and the flow direction during normal operation of the cryolink.

<u>Normal operation:</u>

1. The tower containing the mirror is vented. Tower valve V1 is closed.
2. Close ITF arm valve V2.
3. Bake-out of ITF arm, while the arm is pumped by a turbo-molecular pump. Bake for 1 month at 150° C.
4. Fill the cryolink with LN2.
5. Pump-down of mirror tower (V1 remains closed). It takes about 2 days to reach 10^{-7} mbar (really?).
6. Open V1, keep V2 closed.
7. Open V2.

8. Isolate turbo-molecular pumps. Start ion-pumps.

Fig. 24 shows the control settings during regeneration of the cryolink.

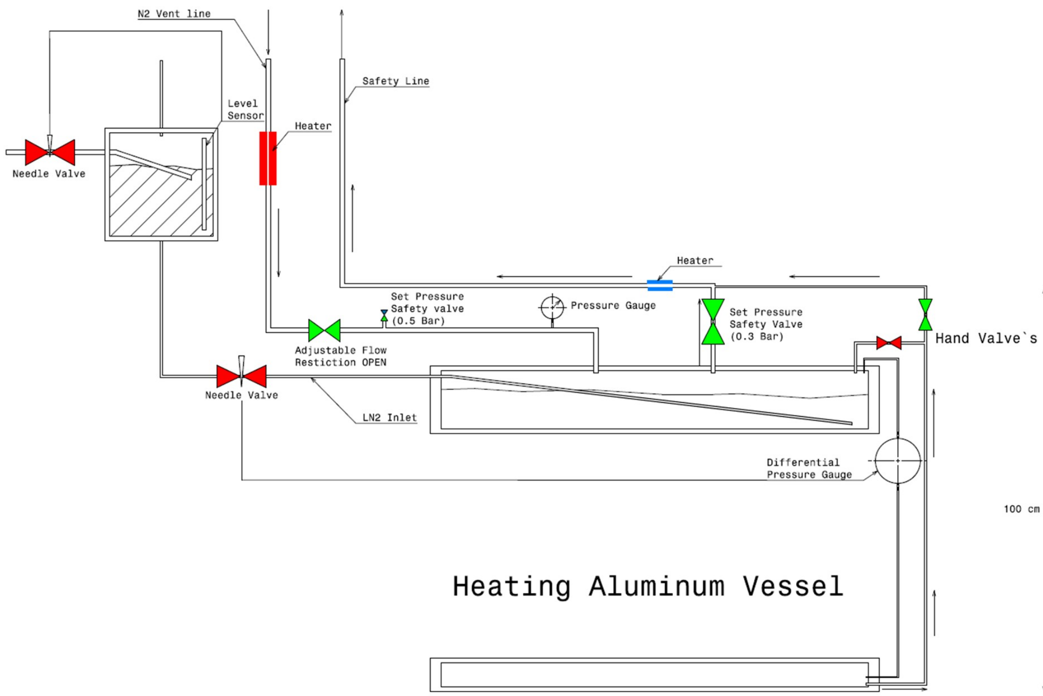

Figure 24: Schematic representation for the control settings of various valves and the flow direction during regeneration of the cryolink.

<u>Regeneration:</u>

1. During normal operation the LN2 level is at 950 mm. LN2 is filled and GN2 is vented.

2. Empty cryolink by opening valve CV1 on cryolink. Close valve CV2 and restrict the opening of needle valve CV3. In this manner pressure is build up in the cryolink. The pressure can be monitored on the differential pressure gauge.

3. When the pressure difference exceeds about 0.08 bar (note that this corresponds to $\rho h \approx 0.8$ kg/l $\times$ 1 m), the LN2 will leave the cryolink.

4. Continue until the cryolink is empty.

5. Admit heated GN2 through valve N2 in order to heat-up the cryolink. This gas exits through valve CV4 (and also CV1).

6. When the entire cryolink reaches a temperature of 150° C, the procedure is completed (this should take about 6 hours).

Fig. 25 shows the control settings during venting of the cryolink.

The above procedures should be worked out in detail and the corresponding software for the PLC should be developed. Subsequently, these procedures should be tested with the cryolink prototype set-up.

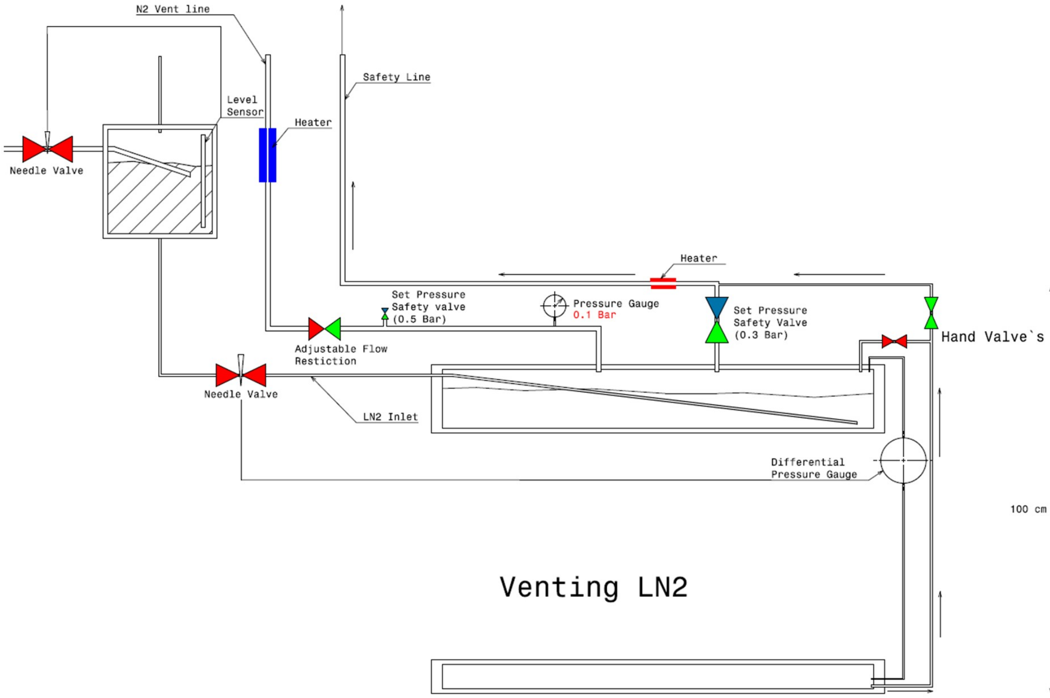

Figure 25: Schematic representation for the control settings of various valves and the flow direction during venting of the cryolink.

2.2.4 Sub-task: Cryogenic control system design

A preliminary outline for the cryo-control system is given in Fig. 26. Cryogenic sensors will be

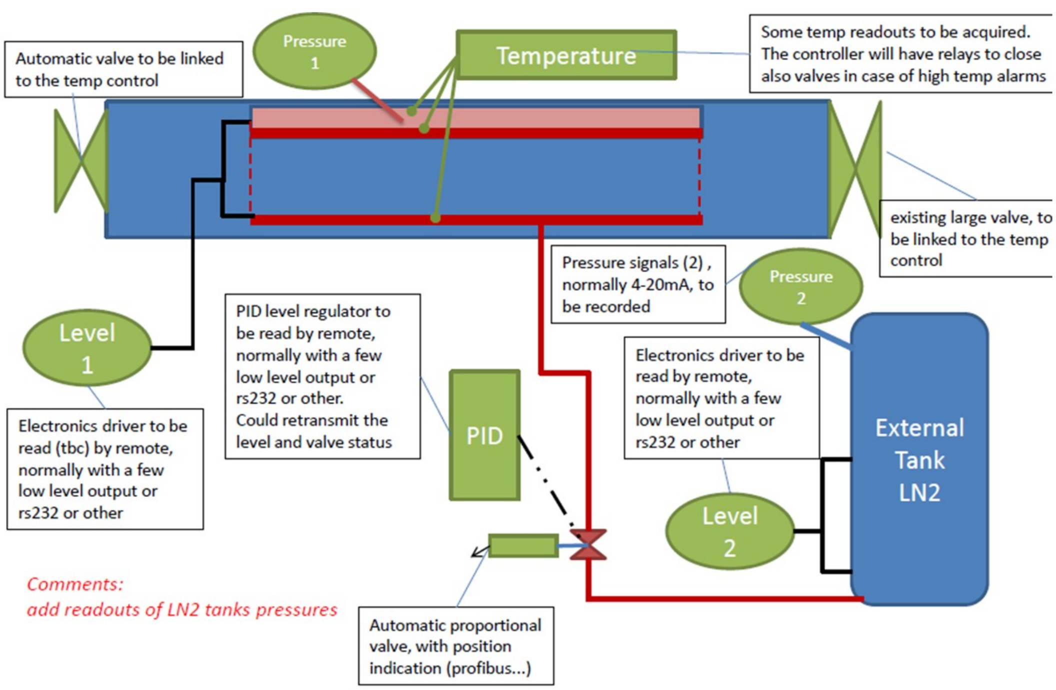

Figure 26: Sketch of the cryo control system for the cryolink. The cryo system is identical for all links.

used to monitor the temperature distribution and the LN2 levels in the cryostat. The controller will have relays to close valves in case of high-temperature alarms. An automatic proportional valve will be used to control the LN2 flow from the external LN2 storage tank into the cryolink. A PID level regulator will be remotely read-out for example with a RS232 connection.

The entire system needs to be available at Nikhef for prototype tests.

It remains to be studied how the above system integrates with the phase separator.

Four of these systems need to be developed for all cryolinks and installed at the EGO site. The cryo-control system has to be integrated with the Virgo slow-control system.

2.2.5 Sub-task: LN2 supply system and transfer lines

Factors considered in the selection of the most suitable liquid nitrogen distribution system are ease of fabrication and handling, reliability, safety, and, of course, cost (both initial investment and running costs, including maintenance). The adopted reference design is a 'standard' distribution plant based on large storage vessels (one for each cryolink) and vacuum insulated transfer lines. The lines could also include a multilayer superinsulation to reduce heat leaks and inner bubbling. The estimated overall heat leak for each cryotrap including transfer lines is in the range of 300 W. Typical losses for a 30 m long line with an insulating vacuum of 10^{-2} mbar are estimated to be 50 W or less [16, 17]. Losses of a good quality storage vessel are typically in the range of 1% per day of its content. Taking some extra safety factor we can estimate an upper limit for the overall heat load of 700 W/trap (for 10,000 l vessels) [19], corresponding to a liquid nitrogen consumption of 350 l/day per trap, and to 1400 l/day for the four traps. With these consumption rates the refilling of the exhausted LN2 should occur once per month.

The transfer lines could also include an intermediate annular pipe for collecting cold vapor to reduce heat leak into the LN2 (see Fig. 27). The system allows for rapid disposal of LN2

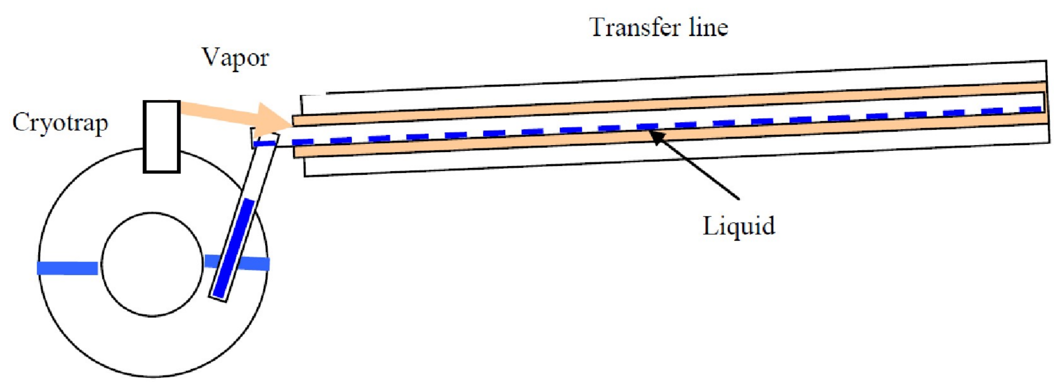

Figure 27: Schetch of the LN2 supply system. The transfer line contains a path for nitrogen vapor to reduce the heat leak into the liquid.

and the circulation of heated GN2 through the cryolink (necessary during regeneration since it significantly shortens the process time). INFN Genua is responsible for providing transfer lines at the EGO site. Being standard plants their safety and reliability should be ensured.

Nikhef will provide transfer lines and a Dewar in order to allow testing of the prototype at the Nikhef site. Note that about 500 l LN2 are needed for cooldown of a cryolink (about 1 l LN2per kg of aluminium when using the latent heat of evaporation, and 0.64 l LN2 per kg when also using the enthalpy of nitrogen [18]), while normal consumption is estimated at about 350 l/day.

2.2.6 Sub-task: Phase separator

A phase separator will be used to separate LN2 from GN2 (nitrogen in the gas phase). Note that LN2 has a volumetric expansion factor of 700 to GN2 at a temperature of 300 K. In general the expansion in the cryolink is to lower temperatures and a more modest expansion factor of 175 is often adequate (80 K). A preliminary design of this system is outlined in Fig. 28. The phase

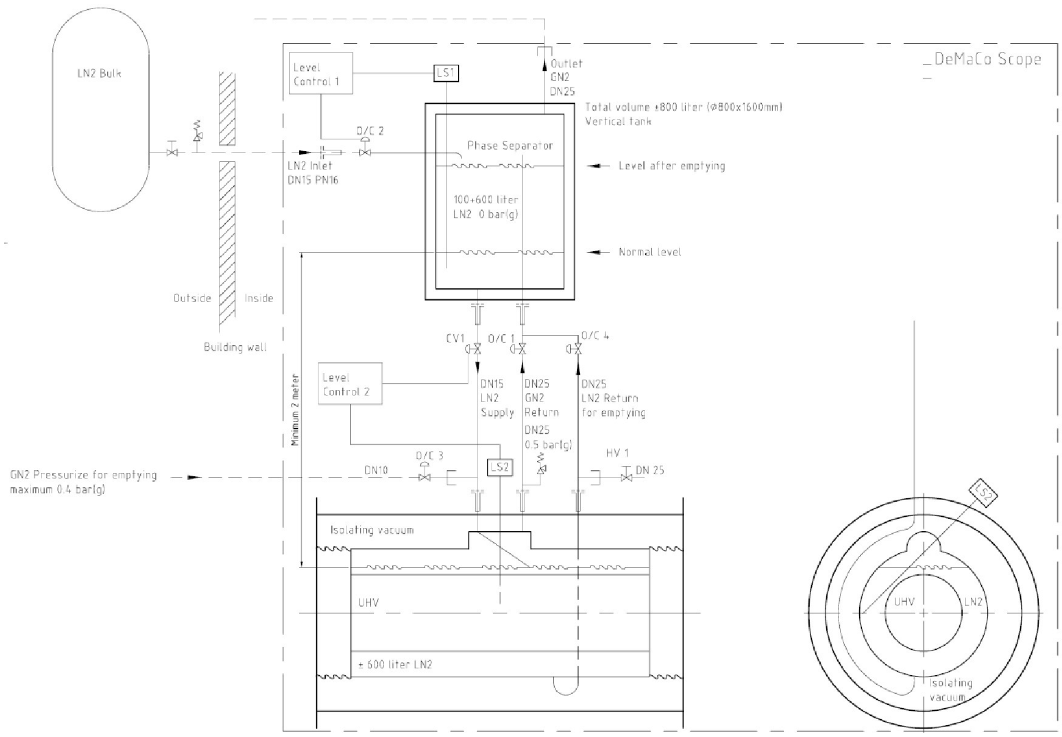

Figure 28: The phase separator with control system for each cryolink.

separator is vacuum isolated and has a total volume of 800 liters. The normal effective volume of LN2 is 100 l and there is buffer volume of 600 liter LN2 for emptying the cryolink (needed).

The phase separator is equipped with a open/close filling valve and a capacitive LN2 sensor that provides a 4 - 20 mA signal. The level controller (DC206) will be situated in a central electrical switching cabinet that opens and closes the filling valve at the start and stop filling levels, respectively.

The phase separator will be placed about 1 - 2 m in height above the cryolink. The phase separator is equipped with two supports that can be used to fix it to the outside world. The separator will have Johnston couplings for connections to

- the filling line from the LN2 buffer vessel;
- the filling line to the cryolink;
- gas purge line to the outside;
- gas return line of the cryolink.

2.2.7 Sub-task: Bake-out system for Virgo interferometer arms

Bake-out equipment is already existing and installed in Virgo. No construction costs have to be sustained, apart for consumables: fuel and power generators to be rented during bake-out period. The estimated cost is 300 kEuro to bake both tubes and we do not consider additional costs for Advanced Virgo. Bake-out of the ITF arms could be performed in a second step, when convenient for the commissioning activity, allowing a simpler start for the vacuum system together with a favourable distribution of the manpower and of the economical effort. Thanks to the cryotraps, a base pressure around 10^{-8} mbar will be obtained in the ITF arms without baking, allowing a first period of interferometer commissioning. When required, both arms will be baked during a stop lasting 2 months.

2.2.8 Sub-task: Enlarged links

The links (vacuum tubes) connecting the various towers in the Central Building have to be replaced for different reasons:

- the positions of the towers will be changed by up to one meter along the beam direction;
- the clear apertures of the links have to be increased since:
  1. the average radius of the beam in the central zone will be 60 mm, instead of the present 21 mm;
  2. the optical lay-out of the interferometer may require a clear passage for multiple beams between the towers, in order to accommodate the non-degenerate recycling cavities and widely separated pick-off beams, as produced by large wedge angles in the mirrors.

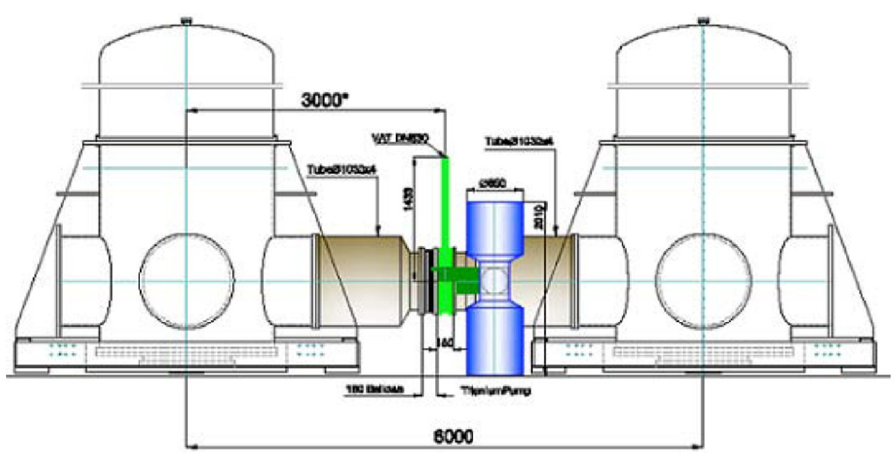

Figure 29: Enlarged link baseline design.

The length of the six links will range between 2 and 4 m, including bellows to allow thermal expansion and, possibly, valves to separate the towers. We consider a general scheme of links of 1 m with or without 650 mm valves (see Fig. 29) that is adaptable to the baseline optical design. The largest possible diameter is 1 m, given the size of the corresponding ports on the towers. Glass baffles will not be installed, since the large diameter would imply more than ten fragile narrow baffles per link; stainless steel baffles could be used instead, as in the ITF arms, while parasitic beams will have to be caught by suitable glass traps.

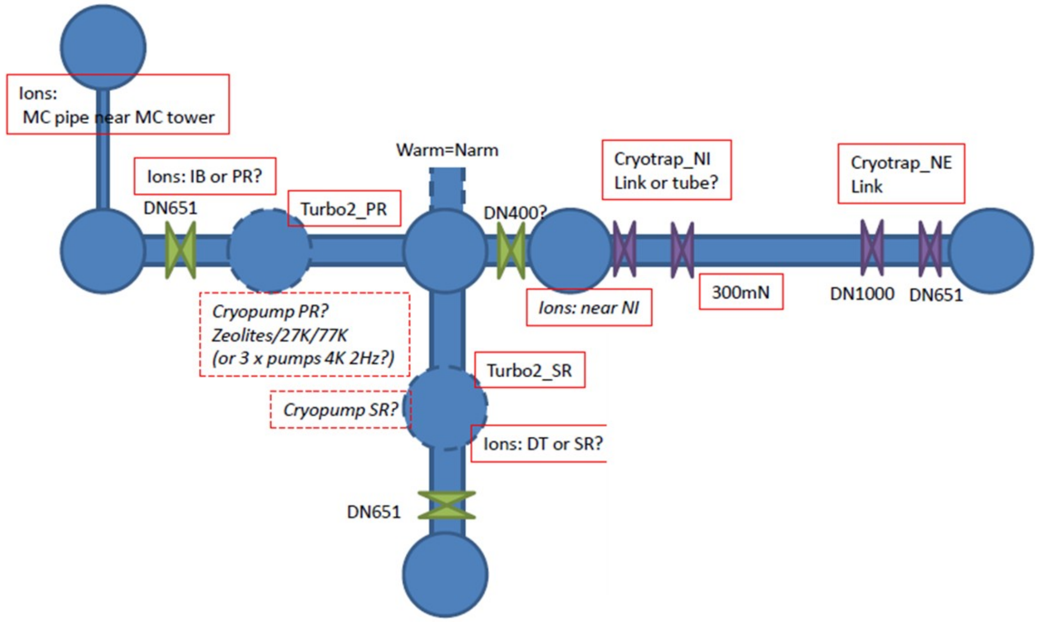

Figure 30: Enlarged link baseline design.

A preliminary design of the central vacuum system is shown in Fig. 30. The towers that house signal recycling (SR) and power recycling (PR) optics will be permanently connected to the tower that houses the beam splitter (BS). A total of 5 ion-pumping stations are used in running conditions. These stations are positioned near the input bench (IB), the detection bench (DB), the mode cleaner (MC), the input mirror towers for both the North arm (NI) and the West arm (WI), or PR and SR, depending on the link geometry (a nominal pumping speed of 5000 l/s will be used). It is expected that the gas load from the bench towers will increase to xxx mbar l/s. Two large (4000 l/s) turbo-molecular pumps will be used during commisioning.

The present baseline solution[5] requires a total of 2 valves with 800 mm diameter, and 2 (+ 1 spare) with 650 mm will be ordered and procured by Nikhef. This represents a significant cost item and must be handled with great care.

The valves will need the following modifications with respect to 'standard' VAT options:

1. a custom-made flange design is needed that matched the flanges used on the links and that allow the use of metallic gaskets (normally of the helicoflex type);

2. a metal seal should be used on the bonnet and all other parts except for the gate. There the seal shall be made of Viton;

3. custom degassing treatments were carried out on the existing 1 m diameter Virgo valves on the Viton and on the metallic part of the valve body. It remains to be discussed if this is necessary or not;

4. we need to discuss with VAT to reduce the mechanical shock on the valves during closing (one way could be just by limiting the driving air flow?);

5. some of the valves will be equipped with viewports on the gate in order to allow for alignment operations with part of the towers in air.

[5]This baseline solution is at present uncertain and almost ruled out.

2.2.9 Action items

1. Redo the vacuum simulations for the final prototype design. The results will be compared to measurements on the prototype. The simulation results for LN2 consumption will be compared to the performance of the prototype (2 weeks).
2. Prepare a detailed regeneration procedure (2 weeks).
3. Design cryolink vacuum system and define interaction with control system (2 weeks).
4. Define various modes of operation of cryolinks (2 weeks).
5. Develop in collaboration with EGO the PLC routines (4 weeks).
6. Test PLC routines on prototype (2 weeks).
7. Design cryolink cryo system and define interaction with control system (2 weeks).
8. Design integration of phase separator (2 weeks).
9. Established whether the buffer volume of 600 liter LN2 for emptying the cryolink is needed (2 weeks).
10. Prepare dewar and transfer lines for prototype (2 weeks).
11. Specify number and type of valves (1 weeks).
12. Procurement and quality control for the valves (1 day/2 weeks during fabrication).
13. Installation of position sensors, micro-switches. Development and integration in EGO control system (4 weeks).

2.3 Task: Thermal modeling

2.3.1 Sub-task: Thermal effects on interferometer mirrors

The proximity of large surfaces cooled to liquid nitrogen temperature will induce thermal effects on the mirrors through radiative heat exchange. The relevance of these effects, in terms of structural and optical curvature of the mirrors, has been analyzed independently by the Nikhef and Roma Tor Vergata groups with finite element thermo-mechanical simulations. Figure 31 shows the 3D model of the setup made with COMSOL. The inner diameter of the cryolink is

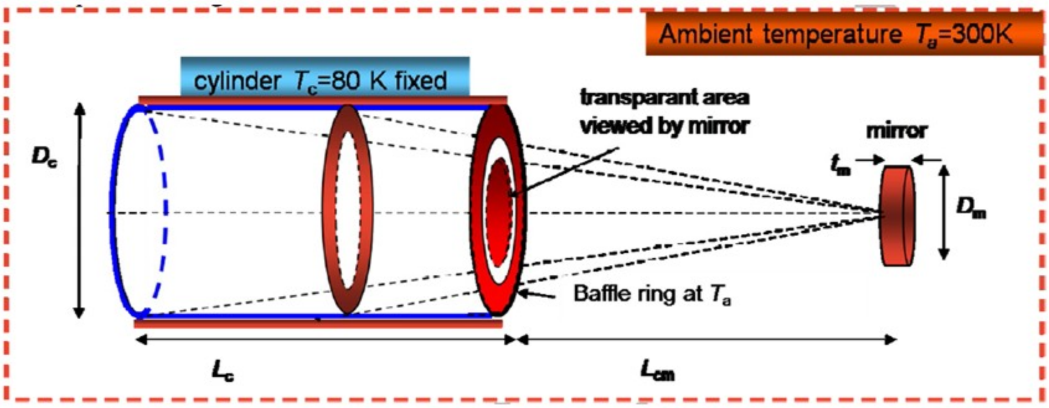

Figure 31: The 3D finite element model used to estimate thermal effects on Virgo mirrors.

denoted D_c, while L_c represents the length and L_{cm} the distance between the cryolink and the mirror. The diameter and thickness of the mirror is denoted by D_m and t_m, respectively. Two different solutions have been modeled and analyzed, and the corresponding geometries are shown in Figure 32:

- a cryolink with a diameter of $D_c = 0.65$ m;
- a larger cryolink (1 m in diameter) with baffles along its length.

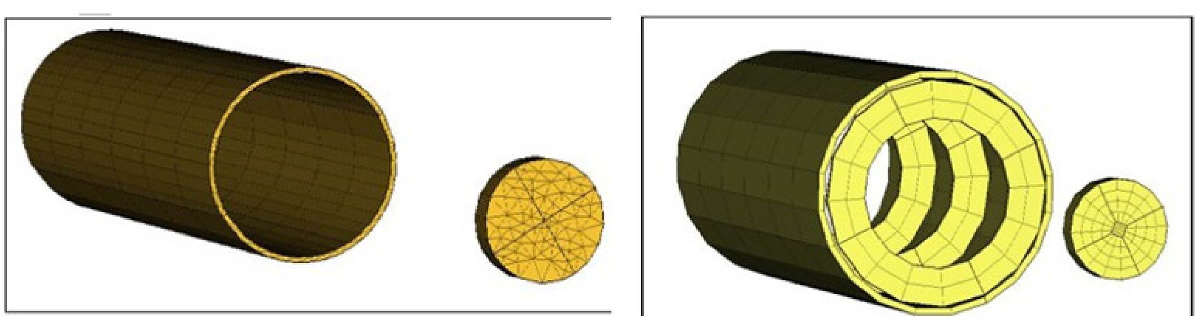

Figure 32: Left figure: a 0.65 m diameter cryolink with no baffles. Right figure: a 1 m diameter cryolink with baffles.

The results of the simulations are summarized in Table 2.3.1 as function of the cryolink diameter and the presence and position of the baffles. The power emitted by the mirror towards the cryolink is denoted by P_M, while T_m represents the temperature decrease of the central part of the surface of the mirror facing the trap. The radius of the equivalent lens in the thin-lens approximation is represented by $R_{\text{thermo-optical}}$.

D_c $[m]$	baffles	P_M $[W]$	ΔT_m $[K]$	$R_{\text{thermo-optical}}$ $[km]$
0.65	no	0.42	0.21	120
1.00	no	0.80	0.43	60
1.00	b_1	0.24	0.12	220
1.00	$b_1 + b_2$	0.23	0.11	250
1.00	$b_1..b_3$	0.31	0.16	170
1.00	$b_1..b_4$	0.40	0.19	100
1.00	$b_1 + b_4$	0.44	0.21	120

Table 2.1. Summary of 3D FEM results.

Note that the Roma Tor Vergata group analyzed the system with a 2D axi-symmetrical model with ANSYS. There is only one baffle, with a diameter of 60 cm, placed 10 cm away from the trap to reduce diffused light noise. The output of the FEM model has been used to evaluate thermal effects in terms of the Optical Path Length (OPL) increase and change in the Radius Of Curvature (ROC) of the test mass (TM). Figure 33 shows the OPL increase due to the trap compared to that due to the YAG power absorbed by the TM. Note that the curvatures of the two OPLs are opposite and that the absolute value of the trap OPL is small compared to that of the YAG. The change in the ROC has been evaluated to be of the order of 2 m, small compared to an absolute value of the ROC of about 1500 m. This change is again going in the opposite direction of that due to the YAG absorption.

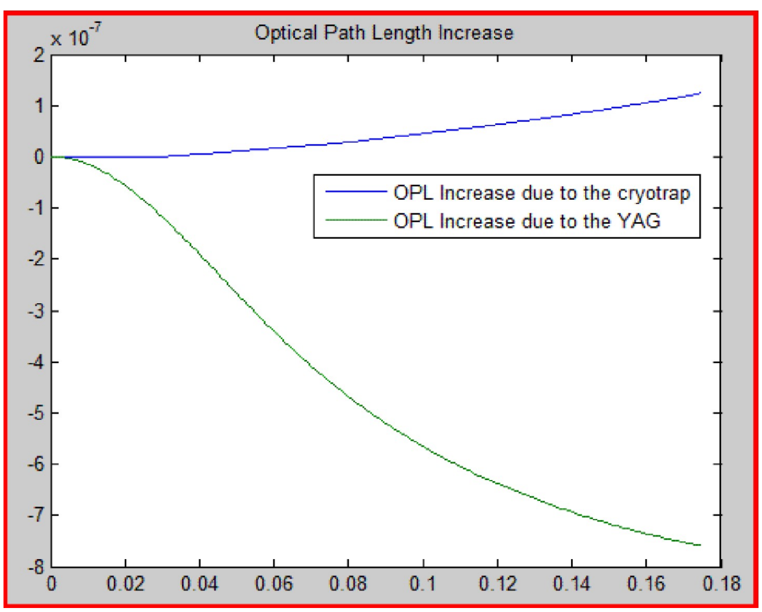

Figure 33: OPL increase due to thermal effects in the TM. The upper curve represents the OPL due to the trap, while the lower curve shows the OPL increase due to the absorption of YAG power.

2.3.2 Sub-task: Thermal modeling of cryolink

The heat load on the cryolink is mostly due to radiation. Radiation from the sides is minimized by a system of xxx radiation shields (superinsulation is not used, since we would like to have the option to bake the cryolinks at temperatures up to 200° C. Although this may be accomplished with kapton-based superinsulation, we believe that the use of metal screens presents a more robust engineering solution.). Front and back of the cryolink are open to 300 K radiation and this constitutes the dominant heat source. Note that heat leaks through suspension and bellows can be neglected.

Finite-element analysis (FEA) has been performed to estimate the thermal performance of the cryolink. Important input for the thermal simulations is the emissivity of the surface of the link. Since this surface will be covered with a layer of frozen water, the emissivity will be time dependent. Fig. 34 shows the emissivity of a water coating versus thickness. We expect for a

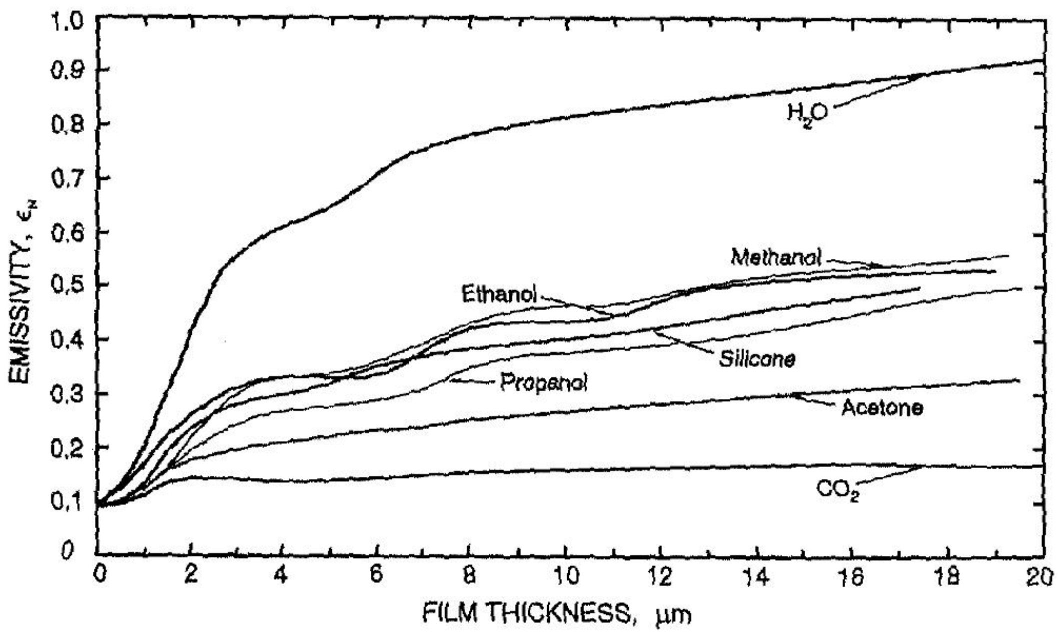

Figure 34: Emissivity of polished stainless steel at 77 K versus film thickness of various frozen gases.

clean trap an initial emissivity of about $\epsilon \approx 0.1$. After about one year of operation a 1 - 2 μm thick layer has built up and ϵ has increased to about 0.3. FEA predicts an initial heat load of xxx W, which increases to xxx after about one year of operation.

2.3.3 Action items

1. Redo simulations of thermal effects on Virgo mirrors for final geometry of the cryolink and baffle system (2 weeks).

2. Redo thermal finite-element analysis of the cryolink (2 weeks).

2.4 Sub-task: Optical modeling of diffused radiation

The criteria applied in Virgo to moderate diffused light contributions will be applied also to the desin of the cryolinks:

- the minimum free aperture radius is about 5 times larger than the average beam radius;
- any discontinuity (potential reflecting spot) of the vacuum enclosure is hidden by suitable absorbing glass baffles, with respect to the beam spot on any mirror;
- no point of the smooth surface of the vacuum enclosure can be seen by the beam spots on two facing mirrors.

Moreover, in the main part of the arm tubes, between two large valves, all the inner surface is hidden by conical stainless steel baffles, with respect to the beam spots on the mirrors. This configuration has proven to be largely safe for Virgo. We have chosen a similar configuration

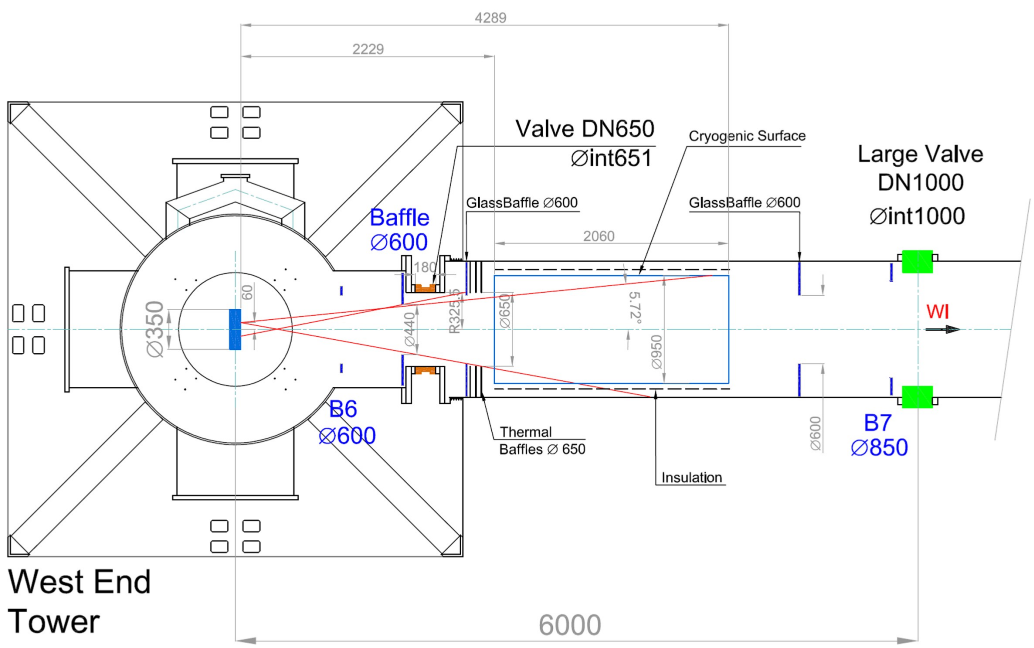

Figure 35: Proposed baffle configuration for the cryotrap. Glass baffles with diameters of 600 and 850 mm are employed.

(see Fig. 35) for the cryotrap. The size of the additional valves and position and diameter of baffles will be optimized with respect to diffused light.

Vinet evaluated the backscattering noise [8] from the cryolinks. He assumed a length of 1.5 m and a diameter of 0.9 m. The entrance of the link was 2.75 m from the mirror and the cryolink was made from stainless steel. The backscattering rate from stainless steel is known [9] and amounts to

$$b(\theta) = 0.83e^{-5.5\theta}, \tag{19}$$

where θ is the angle of incidence. Seismic excitation with spectral density $\eta(f)$ of longitudinal random motion (along the optical axis) of the cryolink, causes phase noise $n(f)$. For a weak modulation depth, we have

$$n(f) = \frac{2\sqrt{2}}{\lambda}\eta(f). \tag{20}$$

The angular distribution of light scattered by the mirrors can be modeled as

$$p(\theta) = \frac{\kappa}{\theta^2}, \tag{21}$$

and the integrated scattering being denoted by ϵ, we have for 10 ppm losses $\epsilon \times \kappa \approx 10^{-7}$.

The power spectral density $h(f)^2$ due to backscattering noise from an element of the cylinder located at z and of angular width $d\theta$ at angle θ from the mirror, can be computed as

$$dh(f)^2 = \frac{\lambda^4\epsilon^2}{64\pi^4 L^2 z^2} p(\theta)^2 d\Omega b(\theta) n(f)^2, \tag{22}$$

with L the length (3 km) of the cavities, and $d\Omega = 2\pi \sin\theta d\theta$ the solid angle of the element as seen from the mirror. Note that $\theta_i = \arctan a/z_i$. Integration gives

$$dh(f)^2 = \frac{\lambda^4\epsilon^2\kappa^2}{32\pi^3 L^2 a^2} \int_{\theta_1}^{\theta_2} \frac{b(\theta)\sin^3\theta d\theta}{\theta^4\cos^2(\theta)} n(f)^2 d\theta \quad \rightarrow \quad h(f) = \frac{\lambda^2\epsilon\kappa}{La}\sqrt{\frac{0.9B_0}{32\pi^3}} n(f), \tag{23}$$

with $B_0 = 1.47 \times 10^{-4}$.

Substituting the parameters, we find $h(f) \approx 3 \times 10^{-26}\ n(f)$ and in the low excitation regime where $n(f) \approx 0.084 \left[\frac{10\ \mathrm{Hz}}{f}\right]^2$ Rd Hz$^{-1/2}$ this yields

$$h(f) \approx 2.5 \times 10^{-27} \left[\frac{10\ \mathrm{Hz}}{f}\right]^2 \mathrm{Hz}^{-1/2}. \tag{24}$$

Thus, Vinet has shown that a cryolink diameter of 0.9 m presents an acceptable solution, when scattering centers on the various baffles visible by the laser beam are smaller than $A \leq 1\ \mathrm{mm}^2$. Therefore, glass baffles are used where the surface has been provided with an anti-reflection coating.

2.4.1 Action items

1. Develop a scheme for the baffles system and minimize their movement due to both seismic effects and noise from bubble excitation (also see Task xxx).
2. Establish whether it is possible to have a direct sight from the mirrors to the cold surface of the cryolink for angles greater than 0.1 rad.
3. Develop support system for the baffles. Note that about 50 mm of space is needed for installation of a baffle. Glass baffles can be supported by flexible stainless fingers which can be welded to the inner board of the vacuum vessel.
4. The baffles will cool down during LN2 operation because of thermal radiation exchange. The contraction should be minimized. Measurements should be carried out on the prototype. Perhaps Nikhef's Rasnik system can be used for this.
5. Establish whether stainless steel baffles can be used.
6. Test the operation of a glass baffle in a cold cryolink environment (Task xxx).
7. Vinet's calculations employ a transfer function of unity between the floor and baffles and assume a seismic noise spectrum of $h = 10^{-8}\left(\frac{10\ \mathrm{Hz}}{f^2}\right)$ m/$\sqrt{\mathrm{Hz}}$. Finite element analysis needs to be carried out on the cryolink cold vessel in order to estimate the actual transfer function. Damping may be incorporated to suppress resonances (2 weeks).

8. Perform measurements of the various transfer functions on the prototype.

9. The beam and also no stray beams should hit the surface of the glass baffles. It is estimated [**?**] that when the beam (xxx W) is incident on 1 mm^2 mm of glass surface, a temperature of 800° C is reached in 1 minute. Check this on the prototype with a YAG beam and an infrared camera. This will result in thermal shock and breaking of the baffle. It must be encertained that this cannot occur, *e.g.* when beam is lost during tuning or commissioning.

2.5 Sub-task: Cryolink prototype and test protocol

As soon as the main dimensions (length L and diameter D) are frozen, a cryolink prototype will be designed and constructed. The full-scale prototype will be equipped with a realistic vacuum system (see Task xxx), control system (Task xxx), slow-control system (Task xxx), phase separator (Task xxx) and transfer line (Task xxx). Liquid nitrogen will be provided from a xxx l dewar.

2.5.1 Action items

1. The front-end of the prototype will be equipped with a gas-inlet system. Nitrogen consumption will be measured with a xxx gas meter. In addition, temperature, pressure and partial pressure sensors will be installed.

2. The cryolink will be equipped with a bake-out system consisting of heating tapes, rockwool insulation and an aluminum cover. A PLC (type xxx) will be used to control the bake-out sequence and is provided with information from temperature sensors. Data are logged with a Labview application.

3. Vibration analysis is performed by exciting the system at various locations, while measuring the response with accelerometers and velocity sensors. In this manner the relevant transfer functions can be obtained. Impulse excitations allow to determine Q-values of the various suspension systems.

4. Test control and slow-control system (2 weeks).

5. Measure LN2 consumption versus surface coverage (2 weeks).

6. Determine parameters for regeneration (2 weeks).

7. Develop PLC software (in collaboration with EGO) and debug (6 weeks).

8. Study possibility of direct optical measurement of ϵ (2 weeks).

2.6 Sub-task: Risk analysis and safety issues

Risks are related to the opening of the 3 km vacuum tubes, cutting out and reinstalling 4 cryolink modules several meter long (handling difficulties, pollution, leaks, involvement of external companies in the installation plan). The following major risks can be identified:

1. **Vacuum contamination after baking**

   Basic risk is the spoiling of vacuum level in tubes once baked. In the most severe case one should repeat the bake-out (if pressure level increase up to high value, *i.e.* like present one). It could happen both during construction or operation, due to a developed leak, or to a wrong operation of the vacuum system or to a failure of some equipment (accidental inlet of air). Probability is reasonably low if right procedure and equipment is adopted . Suitable interlocks will be implemented in the control system to actively protect the system. It is difficult to estimate the residual risk, anyway others baked systems with similar extensions are successfully operated elsewhere.

   Most probably, the bake-out needs to be repeated in case the virgo sensitivity is affected by the event. This constitutes a 1 - 2 month delay for Virgo operations. In addition, manpower and costs are involved.

2. **Control system issues**

   Interference between control system installation phase (when not yet ready) and needed vacuum equipment operations (*i.e.* for testing links or cryotraps)

3. **Leaks**

   Leak on the 2m bottom flange of towers (not accessible one).

2.6.1 Action items

1. Prepare relevant safety documentation for cryolinks. For example strength of reinforcements ribs calculated by FEA. Risk analysis document. Robustness against buckling. Philosophy regarding burst disks, *etc.* (4 weeks).

2. Agree with EGO and Nikhef safety officers that Contractor (*e.g.* Demaco) signs off on the safety issues of the design. Prepare formal CE classification according to pressure-vessel codes.

3. Agree with EGO safety offices on local measures to be taken for cryolinks at the EGO site. For example, installation of oxygen-depletion sensors (1 week).

3 Logistics

3.1 Deliverables

Deliverable 1	Prototype cryolink
Deliverable 2	Cryolinks
Deliverable 3	Cryolink integration

It is appropriate to have a prototype cryolink as first deliverable. This allows for prototype qualification both at the factory and at Nikhef. We have reserved 6 months for this phase. After completion of this phase we proceed with tendering and production of the remaining three units. Here, a total of 12 months has been allocated. For integration of the cryolinks into Virgo we have scheduled a duration of 8 months. Note that several predecessor projects at EGO need to be completed first: the production, firing on site and integration of the larger links, and the displacement of the towers. Installation must be completed at least 4 months before ITF restart, to leave this additional time for re-evacuation of tubes and tests of cryolinks. If bake-out would be considered before the start of AdV commissioning, then the cryolinks installation should be completed 8 months before restart, considering the time needed for the bake itself. Note, that there is no need to vent the interferometer arms.

The cryolinks deliverable includes the following:

1. 4 cryostats, complete with their accessories (*e.g.* heating apparatus for regeneration);
2. cryogenic sensors and their drivers, installed and tested;
3. large vacuum valves for cryolinks;
4. the supporting legs for the cryolinks.

3.2 Involved Virgo subsystems

In the following table we describe the subsystems that are involved in the realization of cryolinks for Advanced Virgo. The subsystems are listed in order of decreasing involvement (# 1 is the subsystem that we intend to modify) describing the typeofconsequence on each subsystem.

Project table 3.1. *The subsystems that are involved in the realization of cryolinks for Advanced Virgo.*

#	Subsystem name	Description of the involvement
1 Cryolinks	OSD	optical constraints for geometry (diffused light issue, *etc.*)
	TCS	thermal effect on input/end mirrors
	PAY	vacuum compatibility of materials
	DAQ	electronics and software compliance
	IME	infrastructure (cable trays, hydraulic pipes, water, *etc.*)

3.3 Involved Nikhef and EGO infrastructure

In the following table we describe the type of infrastructure needed at EGO.

Project table 3.2. *The infrastructure at Nikhef needed for the realization of cryolinks for Advanced Virgo.*

#	Infrastructure	Description of the involvement
	Clean room	Optical glass baffle tests
	Workshop	Cryolink prototype tests
		Cryolink suspension system tests
		Nitrogen two-phase flow tests
	Vacuum department	Prototype vacuum and cryo control systems

Project table 3.3. *The infrastructure at EGO needed for the realization of cryolinks for Advanced Virgo.*

#	Infrastructure	Description of the involvement
	Cryogenics	Transfer lines and LN2 plant
	Clean room	Cryolink installation preparations
	Workshop	Cryolink installation tooling
	Vacuum department	Vacuum equipment
		Vacuum control
	Control	Slow control integration

3.4 Planning

The sequence of construction stages of the cryolinks is:

1. Preparation of specifications documents. Call for tender for the prototype.
2. Contract assignment and executive design
3. Approval of the executive design
4. Prototype qualification and acceptance
5. Production and follow up of the production
6. Acceptance tests and reception
7. Installation at Nikhef
8. Tests at the Nikhef site
9. Repeat steps 1 - 6 for remaining three cryolinks
10. Installation at EGO
11. Tests at the EGO site

The different steps are described below, grouped in three parts: 'finalization', 'production' and 'integration'.

3.4.1 Design finalization, call for tender

preparation of 'technical specification docs':	fall of 2010
call for tender and contract assigned:	end of 2010
approval of the executive design (prepared by Contractor):	early 2011
start of the production:	Q1 2011

3.4.2 Production

The estimated production time for 4 traps is about 14 months (8 months for the first one). The prototype qualification is included in the production phase: the first of the 4 cryotraps shall be completed and qualified in the factory before proceeding with the completion of the remaining 3 units.

1st trap tested in factory:	Q2 of 2011
1st trap tested at Nikhef:	Q4 of 2011
production of the remaining three:	all traps on site at Q2 of 2012

3.4.3 Installation

The installation time is estimated at 1.5 month per trap. In case the installation is made in sequence, a total time of 6 months is involved. During the installation period the interferometer arms will not be available (the large gate valves will be closed). The following constraints can be identified:

1. Installation is schedules for Q3 2012 and shall start after the 'towers displacement', together or following the links installation. The installation of the cryolinks can be handled with same (or similar) tools and manpower (mainly internal) used for 'enlarged links' installation.

2. Installation must be completed at least 2 - 3 months before ITF restart, to leave this additional time for a first running tests of cryotraps.

3. Bake-out could be done after cryotraps have been installed. It will take about 2 additional months, during which the arms are not available (tbc). Baking shall be performed when convenient for commissioning activity , budget and manpower reasons, not necessarily immediately after the traps installation. Mention + 1 month/trap x Firing (on site)?

3.5 Planning and maintenance

Maintenance intervention for the cryolinks is the periodical regeneration, which involves stopping the operation of the interferometer for a few days. Regenerations shall be needed to limit the LN2 consumption, driven by the thickness of the progressively increasing condensed water layer. As shown in Fig. 34 the emissivity varies over time. We do not expect to regenerate the traps more than once per year. A precise regeneration procedure shall be prepared in the next months, as the design progresses.

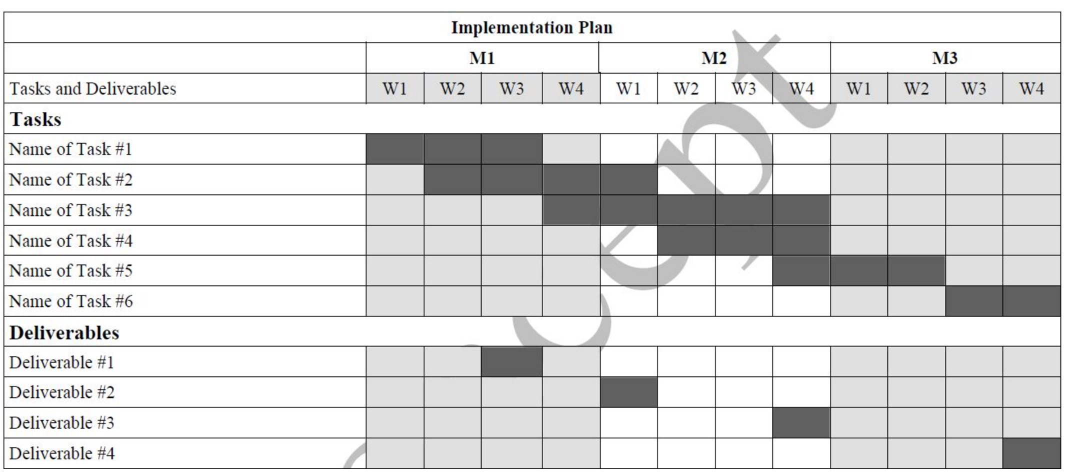

Figure 36: Implementation plan.

In Fig. 36 we show the implementation plan. In addition, the timetable for the deliverables is given.

3.6 Budget

The estimated costs of 'traps' and related accessories is based on budgetary offers received from relevant companies. Taxes are excluded, main spare parts are included. The cost is referred to a cryolink configuration with 650 mm size valves, conservatively. At the present we consider that a 20% contingency has to be added to the quoted costs, in order to compensate for undefined parts of the design.

Following special 'items' are excluded from the EGO VAC budget

1. Infrastructure: needs for the liquid nitrogen supply to be provided outside central and terminal buildings (area preparation, lodgements cabins, electrical power distribution) are not included in VAC and shall be IME.
2. Bake out: the bake-out equipment is already existing and installed in present Virgo. No production costs have to be sustained, apart for consumables: 'fuel' and power generators to be rented during bake-out. It is an approved feature of Virgo and should not considered an additional cost for AdV.

Project table 3.4. *Cost estimate for the realization of cryolinks for Advanced Virgo. The institution responsible for the funding is indicated. Value-added tax is not included. Nikhef numbers are presented in boldface.*

1.1	Cryolinks	four cryolinks	500 kEuro
	Nikhef	external contracts and tools for installation	55 kEuro
		four 650 mm diameter valves	160 kEuro
		modification of valves	40 kEuro
		Total	**755 kEuro**
1.2	LN2 plant	Piping and cryo equipment, 4 units	200 kEuro
	INFN Genua	Concrete instrastructure installation (IME)	40 kEuro
		Total	240 kEuro
1.3	Vacuum equipment	Additional equipment for 4 links	160 kEuro
	EGO	heaters, turbo- and dry-pumps, Ti sublimators	
		RGAs and vacuum sensors for links	80 kEuro
		Total	240 kEuro
1.4	Bake-out		300 kEuro
	EGO		300 kEuro
1.5	Enlarged links	two 800 mm diameter valves	162 kEuro
	Nikhef	three 650 mm diameter valves	80 kEuro
		modification of valves	60 kEuro
		Total	**302 kEuro**

Operative costs have been also estimated: the LN2 supply 0.15 Euro/liter + dewars contract about xx kEuro/year insert costs forecast from sol company.

We have received quotations from VAT for the gate valves. For a diameter of 1000, 800 and 650 (so-called DN630) mm, the price is kEuro 107.5, 80.7 and 39.8, respectively. No VAT is included. Also an expected discount of 7% is not included. The valves need to be N_2 depleted, the gate fabricated from aluminum and the body from stainless steel.

3.7 Manpower

Project issues for construction and installation are summarized in the below table, which reports also the internal manpower needs.

Project table 3.5. *Manpower estimate for the realization of cryolinks for Advanced Virgo.*

Deliverable	Phase	Duration	Manpower
4 cryolinks	Production	14 months	0.5 Mech E
4 cryolinks	Integration	6 months	0.5 Mech E, 1.2 Vac T, 0.1 P

A mechanical engineer shall be needed for half of his time for the production follow-up, while the installation on site shall be performed by one engineer (50%) plus one technician (100%) and an external company for support (handling, dismounting old links and installing new traps with cranes, *etc.*). The external company (2 people) shall be needed for a total period of 12 weeks. About 1.5 months are envisaged to install a trap. In the installation activity is considered also the evacuation (1 week) and the cool-down of each trap (1 week).

Further manpower: a physicist (10%) for baffles positioning and check, and one additional vacuum technician (20%) for special installation activities (pumps installation) and vacuum tests (leak tests).

The LN2 plant installation shall be entirely done by external company under the supervision of a technician (50% during the 4 months foreseen for the installation). Some preparatory activities shall be carried out by the EGO infrastructure team (preparation of external area for LN2 tanks).

Also the procurement of the large valves will require a proper follow-up of the production. Additional manpower effort shall be required.

About bake-out we remark that the apparatus is presently existing and installed in Virgo vacuum system, already operated in the past, when both tubes were baked for the qualificatory tests (2001 - 2002). The manpower need (1 months * 6 FTE per tube?) shall be covered by internal staff, in the hypothesis that bake-out will be performed when principal AdV constructions activities will be over. (Tubes shall be baked when necessary for sensitivity or convenient for commissioning plans).

3.8 Responsibilities

Proposed construction responsibles:

1. Cryolinks — Nikhef
2. LN2 supply plant — INFN - GE
3. Vacuum equipment — EGO

A constant verification of the thermal effects on mirrors is needed not only in the present phase, but also along with executive design and during the phase of tests on site. During the installation phase work and responsibilities shall be normally shared with EGO teams

4 Summary

This project plan describes the realization of cryolinks for Advanced Virgo as we foresee them at this moment. The present insight is based on extensive discussions [20] and in part on the experience with such systems in LIGO and Virgo.

References

[1] '*Phase noise due to forward scattering*', R. Weiss, LIGO-T890025-00-R (1989).

[2] '*Measurement of Optical Path Fluctuations due to Residual Gas in the LIGO 40 Meter Interferometer*', Michael E. Zucker and Stanley E. Whitcomb, LIGO-P940008-00 (1994).

[3] '*Laser beams and resonators*', H. Kogelnik, T. Li, Applied Optics, Vol. 5, No. 10 (1966).

[4] '*Some technical notes on LN_2 boiling*', P. Di Marco, S. FilippeschiR. VIRGO-XXX (2010).

[5] '*Studies on bubble formation in low boiling liquids*', L. Bewilogua, R. Kniiner, and H. Vinzelberg, Cryogenics , February 1970.

[6] '*Influence of Surface Roughness on Transient Nucleate Boiling of Cryogens*', S. Fuchino, N. Tamada, I. Ishii, and M. Okano, Proceedings Proceedings of the Sixteenth International Cryogenic Engineering Confrence/IMCC, Kitakyushu (Japan), 1996.

[7] '*Cryocooler load increase due to external contamination of low-ϵ cryogenic surfaces*', R.G. Ross,Jr., *Cryocoolers* 12 (2003) 727.

[8] '*Backscattering noise from cryotraps*', Jean-Yves Vinet, April 9, 2010. Virgo note.

[9] Jean-Yves Vinet, Phys. Rev. **D** 56, N.10 (1997), p. 6085. Jean-Yves Vinet, Phys. Rev. **D** 56, N.10 (1997), p. 6085. Virgo note.

[10] '*On the problem of scattered light noise from AdV CryoTraps*', Irene Fiori, Virgo note in preparation (2010).

[11] This equation is explained by Fiori as follows: the energy of the peak gets spread over a frequency band up to $f_{\max}$, thus the rms-value reduces by $1/\sqrt{f_{\max}}$. The factor $\sqrt{2}$ seems needed from simulations, although it is not completely understood. In this case, since the scattered vector completes wide (full) rotations (full rotations if $z(t) > \lambda/2$) it seems that the presence of a static phase Φ_0 can be neglected, thus the factor $1/\sqrt{2}$ that we used before, is not needed.

[12] A. Pasqualetti, https://workarea.ego-gw.it/ego2/virgo/advanced-virgo/vac/diffused-light-vs-cryotraps-11feb2010/Kcalc.pdf/ (2010).

[13] '*Diffused light mitigation in Virgo and constraints for Virgo+ and AdV*', B. Canuel, I. Fiori, J. Marque, E. Tournefier, VIR-0792A-09.

[14] '*Back-scattered light noise in Virgo 2nd Science run,* ', I. Fiori, VIR-0029A-10.

[15] '*Glitches from alignment fluctuations and scattered light*', B. Swinkels, presentation VIR-0123A-10.

[16] Based on an emperical relation, $Q \approx 380$ W/(m·Torr. '*Elements de Cryogenic*', R.R. Conte (1970). This amounts to 1 - 2 W/m. INFN-Genua numbers.

[17] Demaco (Cryogenic company in The Netherlands) states 0.4 W/m $\times$ 30 m = 12 W.

[18] B. Jacobs, '*Advances in cryogenic engineering*', Vol. 8, 1963, p. 529.

[19] Storage vessel loss is typically 0.1 - 1.0 % per day. '*Cryogenic Process Engineering*', K.D. Timmerhaus and T.M. Flynn (1989).

[20] Antonio Passaqueti, private communications, May 2010.

Document / Procedure history

Date	Event	Comment
27/02/2009	Start of the procedure	
01/10/2009	Presentation to the AdV review committee	
01/05/2010	Release of the document at Nikhef and EGO	
01/05/2010	Submission to the VSC	

The project has been reviewed in March 2009 by a Virgo internal review committee. The committee came to the following conclusions:

'*Concerning the geometry modification and the related scattered light issues, the analysis carried on shows that the cryolink choice has not a significant impact on this problem. However, we suggest that the analysis on the noise associated to the scattered light should continue and a detailed analysis of the diffraction effect associated to the new geometry has to be done. In addition, some studies should go on in order to identify suitable baffles (material) that could be placed along the cryolink walls.*'

'*We analyzed also a preliminary version of the cryo-mechanical design on the base of which a more realistic estimation of the cost of the hardware has been derived (~1MEuro). Although we consider the proposed design a good starting point, we suggest continuing the comparison with different solutions such as the use of an intermediate thermal shield cooled by the cold nitrogen vapor rather than super-insulation or the use of eccentric vessels. The effort should be devoted to simplify the mechanics and to reduce the thermal input.*'

'*We conclude by listing what it is still missing:*

- *Safety and related equipments are not yet considered.*
- *More details are needed for the nitrogen line transfer design and the automatic fill up system*
- *The Advanced VIRGO plan should be updated by including the small cryotrap solution.*

In conclusion, the reviewers express their appreciation for the high quality work of the Adv VAC team and we strongly support the small trap proposed solution, seen the advantage in terms of cost and time installation.'